J. Fluid Mech. (1996), vol. 319, pp. 219–249

Some shear-layer and inertial modifications to the geostrophic drag on a slowly rising particle or drop in a rotating fluid

By M. UNGARISH

Computer Science Department, Technion - Israel Institute of Technology, Haifa 32000, Israel

(Received 28 December 1994 and in revised form 21 March 1996)

We consider the slow axial motion of a symmetric particle or drop in a bounded rotating fluid for small Rossby and Ekman numbers, Ro and E. Previous investigations pointed out that the available linear-theory results, based on the assumption of a dominant geostrophic core and infinitesimally thin viscous layers, yield a drag force larger than the available relevant experimental results, and are unable to explain some of the observed flow-field properties, for both solid and deformable particles.

Here we attempt to improve the drag calculation model and the interpretation of the flow field by incorporating shear effects in the core (outside the $E^{1/2}$ Ekman and $E^{1/3}$ Stewartson layers), first in the linear ($Ro = 0$) formulation, then with keeping some influential nonlinear inertial terms for small but finite Ro. The major equation for the angular velocity in the core, $\omega(r)$, was usually solved by a finite-differences method, because in the practical parameter range the available analytical results are sufficiently accurate only for a disk particle or for a bubble. Results for various $\varepsilon = (\frac{1}{2}H)^{1/2}E^{1/4}$, no-slip parameter of particle surface κ, and half container height H are presented for both spherical and disk particles. The drag is below the geostrophic value, typically, by 25% for $\varepsilon \approx 0.1$ and by 50% for $\varepsilon \approx 0.5$. The inclusion of the inertial terms causes the lateral ('vertical') shear regions to contract and expand on the upstream and downstream sides, respectively, and an inertial sublayer appears in the latter when $Ro \approx O(E^{3/4})$, but the net contribution to the drag is smaller than expected. Compared with more accurate solutions and experiments the present results underestimate the drag (the reasons are discussed) but are qualitatively consistent in many respects, which indicates that many of the observed flow-field features that have been traditionally attributed to inertial effects (not sufficiently small Ro) are, rather, by-products of the lateral shear (finite value of ε).

1. Introduction

Consider the slow motion of a particle in an incompressible fluid in a container of length $2H^*$ rotating with Ω^* around the axis z, as sketched in figure 1. The particle has fore-aft and axial symmetry and the radius of its circumscribing cylinder is a^*. Let $W^*\hat{z}$ be the velocity of the particle, and ρ^* and ν^* the density and kinematic viscosity of the fluid; an asterisk denotes dimensional variables.

The major dimensionless parameters governing the flow field generated by the motion of the particle are

$$E = T^{-1} = \frac{\nu^*}{a^{*2}\Omega^*},\quad Ro = \frac{W^*}{\Omega^* a^*},\quad \text{and } H = \frac{H^*}{a^*}. \tag{1}$$

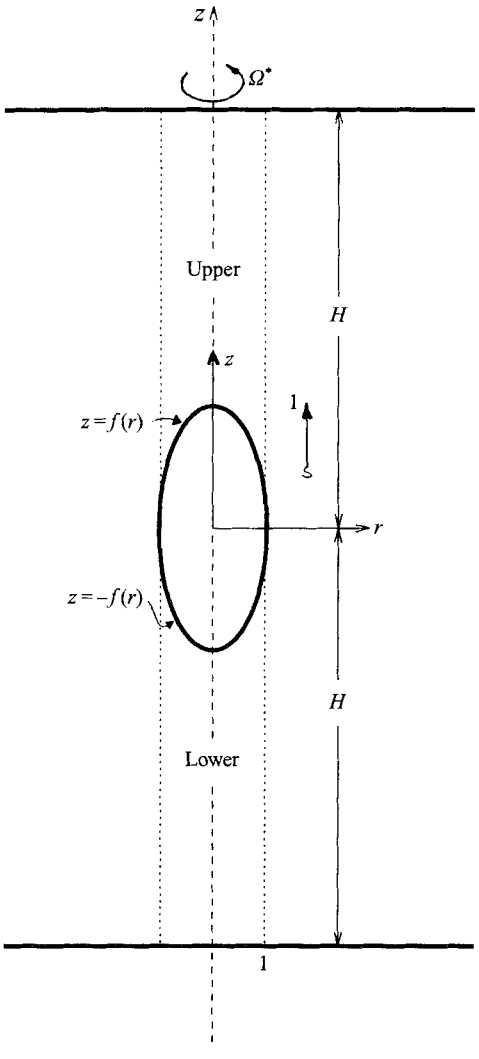

FIGURE 1. Sketch of the configuration. The lengths are scaled with the equatorial radius of the particle, a^*, and the velocities with the rising velocity of the particle, W^*, but $\omega = E^{1/2}v/r$. The cylindrical coordinates system rotates with the rigid 'horizontal' plates and moves with the centre of the particle. See also figure 12.

The Ekman number, E, expresses the typical ratio of the viscous to Coriolis effects in the fluid (the inverse is the Taylor number, T, of the particle). The Rossby number, Ro, a ratio of the convective to the Coriolis accelerations, estimates the relative importance of the inertial nonlinear terms.

The values of E, Ro and H of interest are, respectively, very small, small and moderately large. For example, we would like to consider $E \sim 10^{-4}, Ro \sim 10^{-3}, H \sim$ 5–20, which correspond to some accessible experiments.

For deformable drops the surface no-slip parameter,

$$\kappa = \frac{\beta}{1+\beta}, \tag{2}$$

where $\beta = (\rho^*_{DROP}/\rho^*)(\nu^*_{DROP}/\nu^*)^{1/2}$, is also of importance. It expresses the transport

efficiency of the Ekman layer on the drop interface relative to a similar solid surface, hence $0 \leqslant \kappa \leqslant 1$.† In addition, the Bond number should be specified if the shape function, $f(r)$, is not given, see below.

The available relevant classic theory, developed by Stewartson (1966) and Moore & Saffman (1968,1969), is the linear ($Ro = 0$) approach, by which the flow field has been treated in the asymptotic $E \to 0$ limit as a superposition of z-independent geostrophic 'cores', Ekman boundary layers and Stewartson shear layers on the cylinder circumscribing the *solid* particle.

Recently, Ungarish & Vedensky (1995) solved this linear flow-field problem for a disk particle by transform methods for arbitrary H and E, but no extension of this improved solution to other particle shapes is available.

The drag force, D, which is of major concern in practical applications, turns out to be a still unsolved issue. The well-known dilemma was produced by Moore & Saffman's (1968) prediction, derived under the geostrophic-flow approximation (i.e. without accounting for the Stewartson layers), for a rigid sphere,

$$D_0^* = \frac{43}{105}\pi E^{-3/2}(W^* v^* \rho^* a^*); \tag{3}$$

Maxworthy's (1968) experimental attempts of verification yielded smaller values, typically by 20% for the attained range of small E and small Ro. This discrepancy cast doubts on the usefulness of the linear theory in this problem.

Bush, Stone & Bloxham (1992,1995) made an important extension of the previous asymptotic results to the case of buoyant bubbles or drops in circumstances which allow for decoupling between shape and motion, and derived the corresponding geostrophic drag force formula, which is similar to (3) but with the leading coefficient increasing from 43/105 to 1 as κ decreases from 1 to 0. Bush *et al.* (1995) also performed relevant experiments which, again, show that the actual drag force is smaller than the geostrophic prediction.

The abovementioned experiments also revealed that the velocity field deviates from the geostrophic solution: a radial flux was observed in the interior and the angular velocity measured on the axis was smaller (in absolute value) than expected.

The discrepancy between theory and observations in drag force and other flow-field features was attributed to the neglected nonlinear terms (i.e. not sufficiently small Ro in the experiment; Maxworthy 1968 suggested the value $Ro < 10^{-3}E^{2/3}$ as necessary for compatibility, more than 100 times lower than that attained). However, Barnard & Pritchard (1975) remarked:

> A correction for the effect of the finite thickness of the free shear layers in the theory of Moore & Saffman would almost certainly reduce the discrepancy between the theory and the measurements. Whether this would then lead to satisfactory agreement must await the appropriate calculations.

The idea expressed in this remark is, basically, the motivation of the present research. Two additional related goals are the following. (i) To investigate in a quantitative manner the influence of the inertial terms on the flow field and on the drag when Ro is small. The previous theories provided restrictions of the form $Ro \ll E^a H^b$, where a and b are positive fractions, but did not indicate what modifications appear when $Ro > 0$. (ii) To verify the conjecture that, in the practical range of E and H, the ratio D/D_0 for a disk approximates well this ratio for a sphere (we note that

† In the case analysed in this paper the limit $\beta \to \infty$, i.e. $\kappa \to 1$, recovers the solid particle, but this is not generally correct.

the geostrophic D_0 for a solid sphere is about 18% lower than D_0 for a disk). This conjecture was used ad-hoc by Ungarish & Vedensky (1995) and yielded surprisingly good agreement between the values of D/D_0 given by the 'exact' linear disk solution and the measurements of Maxworthy (1968) for D/D_0 for a sphere at small E and Ro.

To investigate these issues we employ a quasi-geostrophic model, first for $Ro = 0$, then with some inertial modifications. The main assumption is that the $E^{1/3}$ layer is thin, but no such restriction is imposed on the adjacent shear regions (i.e. the $E^{1/4}$ and $E^{2/7}$ 'layers'). This model has in its background the idea that the flow field is typified by the leading terms of a proper asymptotic expansion in the small parameters E and Ro, but the rigour and complexity of such a procedure are simplified here by some looser judgments about the expected leading balances and 'evidence' from related problems. We shall show that the resulting model is quite simple to solve and interpret, and provides important clues to the observed behaviour of the drag and other flow-field features.

2. Formulation

The considered geometry is sketched in figure 1. The cylindrical coordinate system r, θ, z has the origin at the centre of the particle and co-rotates, with constant $\Omega^* \hat{z}$, with the container. The components of the velocity vector, $\boldsymbol{v}$, are $\{u, v, w\}$.

The variables are scaled using the radius a^* of the particle's circumscribing cylinder and the rising velocity W^*, as follows:

$$\{r^*, t^*, \boldsymbol{v}^*, p^*, D^*\} = \left\{a^* r, (a^*/W^*)t, W^* \boldsymbol{v}, \frac{W^* \nu^* \rho^*}{a^*} p, W^* \nu^* \rho^* a^* D\right\}, \tag{4}$$

where p^* is the pressure (reduced by $\frac{1}{2}\rho^* \Omega^{*2} r^{*2}$), D^* is the drag force, ρ^* and ν^* are the density and the kinematic viscosity of the embedding fluid; the asterisk denotes a dimensional quantity.

The equations of motion are

$$Ro\left[\frac{\partial u}{\partial t} + u\frac{\partial u}{\partial r} - \frac{v^2}{r} + w\frac{\partial u}{\partial z}\right] - 2v = -E\frac{\partial p}{\partial r} + E\left(\nabla^2 - \frac{1}{r^2}\right)u; \tag{5}$$

$$Ro\left[\frac{\partial v}{\partial t} + u\frac{\partial v}{\partial r} + \frac{uv}{r} + w\frac{\partial v}{\partial z}\right] + 2u = E\left(\nabla^2 - \frac{1}{r^2}\right)v; \tag{6}$$

$$Ro\left[\frac{\partial w}{\partial t} + u\frac{\partial w}{\partial r} + w\frac{\partial w}{\partial z}\right] = -E\frac{\partial p}{\partial z} + E\nabla^2 w; \tag{7}$$

$$\frac{1}{r}\frac{\partial ur}{\partial r} + \frac{\partial w}{\partial z} = 0; \tag{8}$$

where

$$\nabla^2 = \frac{\partial^2}{\partial r^2} + \frac{1}{r}\frac{\partial}{\partial r} + \frac{\partial^2}{\partial z^2}.$$

Setting $Ro = 0$ in the momentum equation yields the important linear, quasi-steady formulation, which is the main framework of the present investigation, with the anticipation that the results are relevant to practically small values of this parameter. Some modifications for small but non-zero Ro are considered later. The Ekman number E is assumed small (but non-zero).

The particle is considered axi-, fore- and aft-symmetric, i.e. its shape is given by

$$z = \pm f(r), \quad 0 \leqslant r \leqslant 1, \tag{9}$$

and is placed in the midplane of the container, see figure 1. Consequently, *in the linear theory framework* it is sufficient to perform the analysis in the 'upper' or 'upstream' domain $0 \leqslant z \leqslant H$; u, v and p are antisymmetric with respect to the $z = 0$ plane. The midplane symmetry assumption is of course very restrictive from a practical point of view. However, it can be argued that in the range of parameters under investigation the drag is only slightly affected by axial displacements in the range $\pm 0.5H$ around the midplane. This was confirmed by several calculations for off-middle positions (Appendix D), and by the experimental data (T. Maxworthy 1995, personal communication; Bush 1993, figure 5.6).

For a rising drop or bubble (9) requires justification, because in general the shape may be asymmetric with respect to z and may depend on the motion. Bush *et al.* (1995) show that when $Ro \ll 1$† and $g^*/\Omega^{*2}a^* \ll 1$, where g^* is the gravity acceleration, the ellipsoidal shape is dominated by the centrifugal–surface tension balance which is independent of both the axial coordinate z and the flow field induced by the particle's translation. In this case $f(r)$ depends on the rotational Bond number,

$$\Sigma = -\Omega^{*2}a^{*3}(\rho^* - \rho^*_{DROP})/8\sigma^* \tag{10}$$

and can be calculated directly from equation (A3) of Bush *et al.* (1992); σ^* is the interfacial tension. For small Σ the drop is almost spherical.

Thus, $f(r)$ can be considered a prescribed function from the viewpoint of the linear flow-field analysis for either solid particles or drops in a dominant centrifugal field, $g^*/\Omega^{*2}a^* \ll 1$. For non-, fore- and aft-symmetric particles an extension of the present analysis is possible but the details are cumbersome.

3. The quasi-geostrophic model

Obviously, Ekman layers of typical thickness $E^{1/2}$ will appear on the boundaries. In addition, the analysis of Moore & Saffman (1969) produces the following important background points for the present investigation:

(i) On the circumscribing cylinder $r = 1$ 'vertical' inner Stewartson shear layers, of typical thickness $(EH)^{1/3}$, appear. We shall assume that $(EH)^{1/3} \ll 1$.

(ii) Outside the Ekman and the $E^{1/3}$ layers the flow is z-independent. Moreover, owing to the symmetries with respect to $z = 0$ in the present problem, the torque-free particle does not rotate and in the external region $r > 1$ the flow vanishes. Consequently, the boundary condition for v in the region $r < 1$ is $v(r = 1) = 0$ $(= O(H^{-1/6}E^{-5/12})$, while the value in the interior is $O(E^{-1/2}))$.

The equations of motion (5)–(8) in this linear 'quasi-geostrophic' interior are, therefore, approximated by

$$-2v = -E\frac{\mathrm{d}p}{\mathrm{d}r}; \tag{11}$$

$$2u = E\frac{\mathrm{d}}{\mathrm{d}r}\frac{1}{r}\frac{\mathrm{d}}{\mathrm{d}r}rv; \tag{12}$$

$$0 = -\frac{\partial p}{\partial z}; \tag{13}$$

$$\frac{1}{r}\frac{\mathrm{d}}{\mathrm{d}r}ru + \frac{\partial w}{\partial z} = 0. \tag{14}$$

† The practical restriction is $Ro \ll E^{1/2}\rho^*/|\rho^* - \rho^*_{DROP}|$ which is difficult to satisfy in experiments.

The difference between this 'quasi-geostrophic' approach and the extensively used 'geostrophic' approximation is in (12). In purely geostrophic regions the radial motion in the interior is neglected, i.e. u is set zero, and the entire radial volume transport is assumed to be performed by the Ekman layers. However, some prominent and facilitating features of the geostrophic model carry over to the extended model, in particular the z-independence of u, v and p and the essential interaction with the Ekman layers. Moreover, the geostrophic case is a straightforward limiting case (or 'outer' asymptotic solution) of the quasi-geostrophic one. We note that Moore & Saffman (1969) used the term 'viscous Taylor column' for quasi-geostrophic domains.

The importance of the quasi-geostrophic model in the present configuration is in the fact that the angular velocity in the core can be obtained from the solution of a single ordinary differential equation. Letting

$$\omega(r) = E^{1/2} v(r)/r, \tag{15}$$

the key equation, for the upper side $f^+(r) < z < H^-$, $0 \leqslant r \leqslant 1^-$, is

$$2\varepsilon^2 \left[1 - \frac{f(r)}{H}\right] \left(\frac{\mathrm{d}^2\omega}{\mathrm{d}r^2} + \frac{3}{r}\frac{\mathrm{d}\omega}{\mathrm{d}r}\right) - \left[1 + \kappa(1 + f'^2)^{1/4}\right] \omega = 1, \tag{16}$$

subject to

$$\frac{\mathrm{d}\omega}{\mathrm{d}r} = 0 \text{ at } r = 0, \tag{17}$$

$$\omega(r = 1) = 0; \tag{18}$$

The details are given in Appendix A. Unless stated otherwise we consider ω and u on the upper side, and a change of sign is necessary for the lower side.

The parameters entering this equation are

$$\varepsilon = \left(\tfrac{1}{2}H\right)^{1/2} E^{1/4}, \tag{19}$$

which is the e-fold thickness of the classic outer† Stewartson 1/4 layer; κ, the particle surface no-slip parameter, see (2); and H. We shall bear in mind the obvious geometric restriction $H > f_{max}(r) = f(0)$.

Equation (16) is a volume flux balance. The first term represents the transport in the core. The second term is the contribution of the Ekman layers on the horizontal solid boundary and on the particle (the latter is modified by the no-slip factor κ). The right-hand-side term comes from the axial motion which drives (or compensates) the radial volume transport.

We remark that the model (16)–(18) with $\kappa = 1$ was formulated by Moore & Saffman (1969), but has not been implemented in the configurations considered here.

When $\omega(r)$ is known the radial and axial velocities can be readily obtained via (A 7) and (A 9) in Appendix A, and the pressure via (11) with the boundary condition $p(r = 1) = 0$. In particular, the pressure difference yields the drag force, in the direction $-z$, as

$$D = 4\pi E^{-3/2} \int_0^1 |\omega(r)| r^3 \mathrm{d}r. \tag{20}$$

The shear contribution to the drag is smaller, of order E^{-1}, and therefore discarded.

† We use the term 'outer' for the layers that embed the 1/3 'inner' layer.

The *geostrophic* result is the outer solution of (16) in the asymptotic limit $\varepsilon \to 0$, i.e.

$$\omega_0 = -\frac{1}{1+\kappa(1+f'^2)^{1/4}}. \tag{21}$$

The geostrophic result is denoted by the subscript 0 because it can be interpreted as the zeroth term in an expansion in powers of ε. We can readily distinguish two cases:

(i) For inviscid particles, $\kappa = 0$, and for disk particles, $f'(r) \equiv 0$, ω_0 is a constant. The boundary condition (18) evidently requires a boundary layer of thickness $O(\varepsilon)$, the classic outer Stewartson $E^{1/4}$ shear layer.

The geostrophic drag, see (20), is simply

$$D_0 = \frac{\pi}{1+\kappa} E^{-3/2}. \tag{22}$$

Practically, $\kappa = 1$ for the disk geometry, but other values of κ may have some theoretical merits as discussed later. In particular, for $\kappa = 0$ the shape is unimportant.

(ii) For ellipsoidal viscous or solid particles ω_0 varies with r. Since $|f'(r)| \to \infty$ and 0 for $r \to 1$ and 0, respectively, the outer solution ω_0 satisfies both boundary conditions (17) and (18) and the necessity of the shear layer at $r = 1$ is not evident. The typical example is the solid spherical particle, $f(r) = (1-r^2)^{1/2}$, $\kappa = 1$, for which (21) and (20) yield

$$\omega_0 = -\frac{(1-r^2)^{1/4}}{1+(1-r^2)^{1/4}}; \tag{23}$$

$$D_0 = \frac{43}{105}\pi E^{-3/2}; \tag{24}$$

these are the well-known results of Moore & Saffman (1968), whose disagreement with Maxworthy's (1968) experiments cast doubts on the ability of the linear theory to predict realistic flow fields.

It is easily verified that a big portion of the geostrophic drag force is contributed by a thin annulus near the equator. For the solid sphere 29% of D_0 is provided by $0.9 < r < 1$, and an additional 13% is gained in $0.85 < r < 0.9$.

The geostrophic drag depends strongly on the no-slip factor κ, as seen in figure 2. When κ decreases, the contribution of the Ekman layer on the particle to the volume transport also decreases. This is compensated by a larger $|\omega|$ which increases the volume transport in the Ekman layers *on the 'horizontal' solid walls of this bounded configuration.* The decreasing contribution of the particle makes its geometry less relevant to the drag; therefore, as κ decreases, the difference between the drag forces on a disk and on a sphere diminishes.

The major question is how the apparently small, $O(\varepsilon^2)$, shear term in (16) affects the flow fields and, in particular, the drag force. Moreover, we would like to know what happens when ε is not small, in which case the geostrophic approximation is obviously not valid. We emphasize that in the experiments of Maxworthy (1968) and Bush *et al.* (1995) ε was larger than 0.1 and usually smaller than 0.25. In this context it is worth reformulating (A 7), on account of (21), as

$$u = \left(1 - \frac{\omega}{\omega_0}\right) \frac{r}{2[H - f(r)]}, \tag{25}$$

which emphasizes the fact that deviations from the geostrophic ω_0 are accompanied by the appearance of $O(1)$ radial motion in the core.

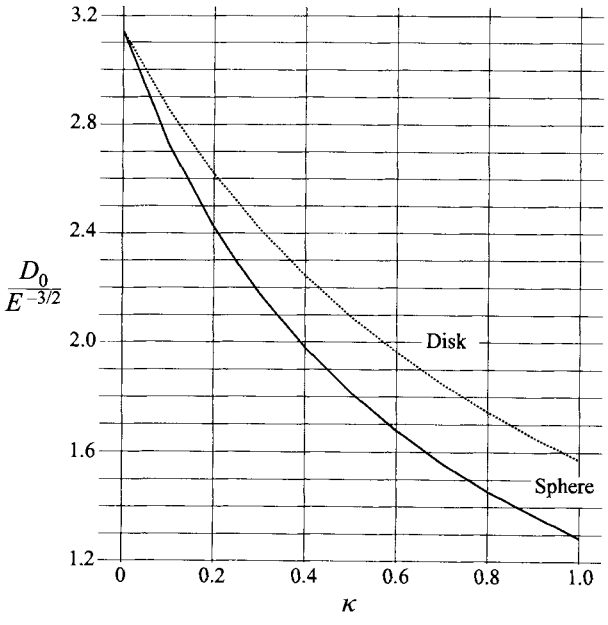

FIGURE 2. Geostrophic drag *vs.* κ for disk and sphere.

We proceed as follows. First, we discuss analytical approaches: when $f(r) \equiv 0$ (a disk) an exact solution to (16) is available, which yields good insight for both small and $O(1)$ values of ε, see §3.1. For $f(r) = (1 - r^2)^{1/2}$ (a sphere) an asymptotic approximation for $\varepsilon \to 0$ is available, but it turns out to be rather useless for practical values of ε ($> 10^{-2}$, say), see §3.2. Next, in §3.3, we discuss numerical results of (16) and (20). In §4 we consider some nonlinear modifications of (16) and (20). Comparisons with other theoretical results and with experiments are discussed in §5.

3.1. *Solutions for the generalized disk and for the inviscid particle; the $E^{1/4}$ layer*

Consider the thin-disk limit of the particle shape, $f(r) \equiv 0$. To facilitate comparison with drops, this disk is generalized in the sense that we allow for (partial) slip on its surface, represented by the parameter κ in (16), although, in practice, $\kappa = 1$ for this geometry. The disk results have convenient mathematical and physical properties and are useful references in this study. The subscript d denotes results for the disk particle. Unless specified otherwise the domain considered is $0 \leqslant r \leqslant 1$, $0^+ \leqslant z \leqslant H^-$.

It is readily verified that for $f(r) \equiv 0$ the exact outcomes of (16)–(18) and (20), for any ε, are

$$\omega_d = -\frac{1}{1+\kappa}\left[1 - \frac{I_1(r/\gamma\varepsilon)}{rI_1(1/\gamma\varepsilon)}\right]; \tag{26}$$

$$D_d = \frac{\pi}{1+\kappa}E^{-3/2}\left[1 - 4\gamma\varepsilon\frac{I_2(1/\gamma\varepsilon)}{I_1(1/\gamma\varepsilon)}\right]; \tag{27}$$

where

$$\gamma = [2/(\kappa+1)]^{1/2}; \tag{28}$$

also, in view of (12),

$$u_d = \frac{1}{2H}\frac{I_1(r/\gamma\varepsilon)}{I_1(1/\gamma\varepsilon)}. \tag{29}$$

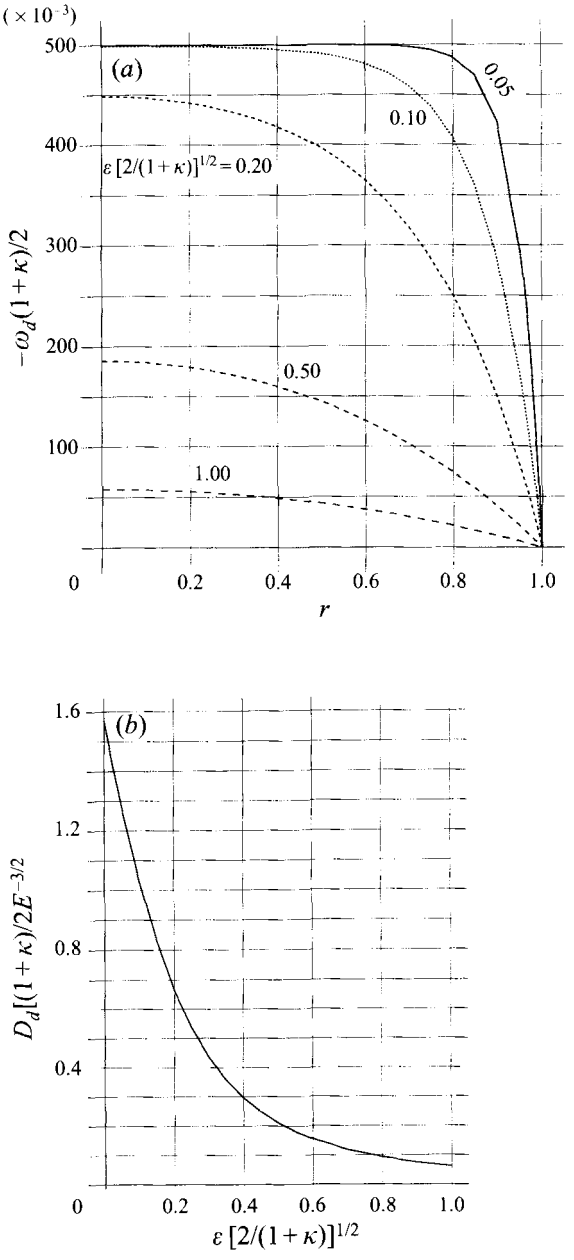

FIGURE 3. Disk: (*a*) angular velocity *vs.* r, for various $\varepsilon[2/(1+\kappa]^{1/2}$; (*b*) drag *vs.* $\varepsilon\ [2/(1+\kappa]^{1/2}$.

Recall the scaling $v = E^{-1/2}r\omega$, i.e. the azimuthal velocities are actually $O(E^{-1/2})$ as compared to the translation velocity of the body.

The behaviour of ω_d and D_d is shown in figure 3. Evidently, the dependency on ε is strong: as ε increases $|\omega|$ becomes smaller than the geostrophic prediction, first near $r = 1$, then for all r. The drag decreases. For further insight, we perform straightforward expansions of the Bessel functions to obtain the following results.

(*a*) For small $\gamma\varepsilon$ (< 0.2, say)

$$\omega_d \approx -\frac{1}{1+\kappa}\left[1-\exp\left(\frac{r-1}{\gamma\varepsilon}\right)\right]; \tag{30}$$

$$u_d \approx \frac{1}{2H}\exp\left(\frac{r-1}{\gamma\varepsilon}\right); \tag{31}$$

$$w_d \approx -\frac{\kappa}{1+\kappa}+\left[\frac{\kappa}{1+\kappa}-\frac{z}{H}\right]\frac{1}{2\gamma\varepsilon}\exp\left(\frac{r-1}{\gamma\varepsilon}\right); \tag{32}$$

$$D_d \approx \frac{\pi}{1+\kappa}E^{-3/2}\left[1-4\gamma\varepsilon(1-\tfrac{3}{2}\gamma\varepsilon+\tfrac{3}{8}(\gamma\varepsilon)^2-\cdots)\right]. \tag{33}$$

Evidently, for $\varepsilon \to 0$ the geostrophic flow results are recovered. The terms associated with the exponent in (30)–(32) represent the 'vertical' $E^{1/4}$ boundary layer, whose thickness (slightly) increases when κ decreases. This layer is obviously needed to satisfy the boundary condition $\omega_d(r=1)=0$. Note the non-monotonic behaviour of the axial velocity: in the geostrophic interior outside the $E^{1/4}$ layer the flux is $O(1)$ toward the particle, but in the layer the flow is $O(1/\varepsilon)$ and from the particle (i.e. the Ekman layer) into the interior (this is best seen by taking $\kappa = 1$ and $z = 0$). The influence of this layer on the drag is very significant, causing the variation $\Delta D_{1/4}/D_0 \approx -4\gamma\varepsilon$.

(*b*) For non-small $\gamma\varepsilon$ (> 1, say)

$$\omega_d = -\frac{1}{8}\frac{E^{-1/2}}{H}(1-r^2)\left[1-O\left(\frac{1}{12\gamma^2\varepsilon^2}\right)\right]; \tag{34}$$

$$u_d = \frac{r}{2H}\left[1+O\left(\frac{1}{8\gamma^2\varepsilon^2}\right)\right]; \tag{35}$$

$$D_d = \frac{\pi}{24}\frac{1}{H}E^{-2}\left[1-\frac{1+\kappa}{32\varepsilon^2}+\cdots\right]. \tag{36}$$

We note that the leading-order terms do not depend on κ; actually, they reproduce a complete core flow, without an Ekman layer contribution, which differs essentially from the geostrophic flow. By using the identity $E^{-2}/H = E^{-3/2}/2\varepsilon^2$ we emphasize the fact that (36) is much lower than the geostrophic prediction (22). The leading terms in (34)–(36) are in agreement with the results for the long container case in the limit of small $(EH)^{1/3}$ obtained by Hocking, Moore & Walton (1979).

Now consider two inviscid particles, $\kappa = 0$, one a disk $f(r) \equiv 0$ and the other an ellipsoid $0 = f(1) \leqslant f(r) \leqslant f(0)$. The formulation (16) for the latter particle differs from that for the disk only by the coefficient $[1 - f(r)/H]$ which multiplies ε^2. We therefore realize that, in general, if $f(0)/H \ll 1$, the inviscid disk solution is an accurate approximation for the inviscid ellipsoidal particle. Moreover, for small ε good accuracy is achieved under the much milder $f(1-\sqrt{2}\varepsilon)/H \ll 1$ requirement because for $r < 1-\sqrt{2}\varepsilon$ the flow is geostrophic, see (30), and independent of the particle-to-wall distance H.

3.2. *Asymptotic solution for spherical particles; the $E^{2/7}$ sidelayer*

For a rigid disk particle the geostrophic outer solution to (16), $\omega_{d0} = -1/2$, does not satisfy the boundary condition $\omega = 0$ at $r = 1$. The appearance of the outer $E^{1/4}$ Stewartson shear layer is obviously triggered by this unmatched condition. On the

other hand, consider a spherical solid particle, $f(r) = (1-r^2)^{1/2}$, $\kappa = 1$ (extensions to other values of κ and other similar shapes is straightforward). Although the geostrophic (outer) solution to (16) satisfies the boundary condition $\omega(r=1)=0$, see (23), a shear layer at $r=1$ must appear.

As indicated by Stewartson (1966), this effect is triggered now by the fact that, as $r \to 1$, $\mathrm{d}^2\omega_0/\mathrm{d}r^2$ grows without limit, hence the first term in (16) must be incorporated in the balance in spite of the small ε. In the physical sense, this means that the shear of ω as $r \to 1$ is large and hence able to support a significant radial motion, $u \sim 1$, in the core. Consequently, the contribution of Hu to the volume transport is commensurate with the flux in the Ekman layers and must be incorporated.

To this end, we consider the spherical particle and r close to 1, and so let

$$x = 1 - r \ll 1;$$

$$f(r) = (2x)^{1/2}(1 - \tfrac{1}{4}x + \cdots); \quad (1+f'^2)^{1/4} = \frac{1}{(2x)^{1/4}}(1 + \tfrac{1}{8}x + \cdots), \tag{37}$$

and substitute in (16) to get

$$2\varepsilon^2\left(1 - \frac{(2x)^{1/2}+\cdots}{H}\right)\left(\frac{\mathrm{d}^2\omega}{\mathrm{d}x^2} - \frac{3}{1-x}\frac{\mathrm{d}\omega}{\mathrm{d}x}\right) - \frac{1}{(2x)^{1/4}}(1 + \tfrac{1}{8}x + \cdots)\omega - \omega = 1. \tag{38}$$

The leading balance in (38) for small x and ε is

$$2\varepsilon^2\frac{\mathrm{d}^2\omega}{\mathrm{d}x^2} - \frac{\omega}{(2x)^{1/4}} = 1, \tag{39}$$

which indicates a boundary layer of thickness $x \sim \varepsilon^{8/7} \approx E^{2/7}H^{4/7}$ in which $\omega \sim \varepsilon^{2/7}$. For a detailed solution of this layer, following Moore & Saffman (1969) we introduce the stretched coordinate s and the rescaled angular velocity G,

$$s = x/A; \quad G = -\omega/B, \text{ where } A = 2^{5/7}\varepsilon^{8/7}; \quad B = (2A)^{1/4}; \tag{40}$$

which reduce (39) to

$$G''(s) - G(s)/s^{1/4} = -1, \tag{41}$$

subject to the boundary conditions

$$G(0) = 0; \quad G(s)/s^{1/4} \to 1 \text{ at } s \to \infty. \tag{42}$$

The solution of (41)–(42), see Appendix B, is displayed in figure 4. For small s, $G(s) \approx 1.01s - 0.50s^2$, and at $s = s_1 \approx 5$ the solution $G(s)$ reaches 98% of its asymptotic value $s^{1/4}$. We therefore can define that the edge of the $E^{2/7}$ layer is, approximately, at $s_1 = 5$, i.e. at $x_1 = 1 - r_1 = 5 \times 2^{5/7}\varepsilon^{8/7} = 5 \times 2^{1/7} \times H^{4/7}E^{2/7}$.

The solution of (16) for a rigid sphere and small ε is now approximated by the following patching: $\omega = \omega_0(r)$, see (23), for $r < 1 - c\varepsilon^{8/7}$ and $\omega = -B\ G[(1-r)/A)]$ for $1 - c\varepsilon^{8/7} \leqslant r \leqslant 1$, where $c = 5 \times 2^{5/7}$ if the boundary layer thickness is defined as above.

The radial motion in the layer, according to (25), is

$$u = \frac{1}{2H}[1 - G(s)/s^{1/4}], \tag{43}$$

which can be compared to (31). For small s, $G(s)/s^{1/4} \sim s^{3/4}$ and $u \approx 1/(2H)$. Thus, like in the $E^{1/4}$ layer on the disk, the major volume transport in the radial direction as $r \to 1$ is performed in the core by the $2\pi rHu$ term, not in the Ekman layers. This

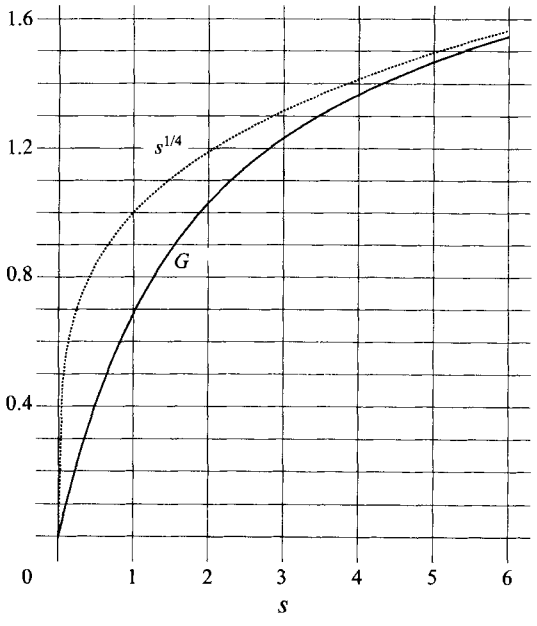

FIGURE 4. $G(s)$ and $s^{1/4}$ *vs.* s in $E^{2/7}$ sidelayer.

can also be noticed in (41): the second term on the left-hand side, which represents the Ekman layer transport, is $O(s^{3/4})$ for small s.

We note that this analysis can be straightforwardly extended to non-rigid spheres, $\kappa < 1$, by taking $A = 2^{5/7}\varepsilon^{8/7}\kappa^{-4/7}$ and $B = (2A)^{1/4}\kappa^{-1}$. The thickness of the layer increases as the viscosity of the particle decreases. Similarly, for a drop, as inferred from Bush *et al.* (1992, Appendix) and Bush *et al.* (1995), the shape is typically modified such that

$$f'^2 \approx \frac{1}{2(1+2\Sigma)x}[1 - 2x(1+2\Sigma) + \cdots]$$

where Σ is the (small and negative) Bond number; therefore A and B should be further multiplied by $(1+2\Sigma)^{1/7}$ and $(1+2\Sigma)^{1/4}$ respectively. The layer becomes thinner because the inclination of the particle near $r = 1$ increases.

Now using (20) we consider the addition to the geostrophic drag due to this layer,

$$\Delta D_{2/7} = -4\pi E^{-3/2}\int_0^{x_1}[\omega - \omega_0](1-x)^3 \mathrm{d}x$$

$$\approx 4\pi E^{-3/2}AB\int_0^5 [G(s) - s^{1/4}]\mathrm{d}s = -4\pi E^{-3/2}AB \times 0.86. \tag{44}$$

Hence, with the aid of (24)

$$\frac{\Delta D_{2/7}}{D_0} \approx -18.6\varepsilon^{10/7}. \tag{45}$$

We notice that for $\varepsilon = 0.13$ the drag reduction predicted by (45) is 100%, which of course is not physically acceptable, so we begin to suspect that the asymptotic analysis of the $E^{2/7}$ layer is restricted to much smaller values of this parameter. In contrast, for a disk the discrepancy between the approximation $\Delta D_{1/4}/D_0 \approx -4\gamma\varepsilon$ and the exact drag reduction obtained from (27) at $\varepsilon = 0.13$ is less than 20%.

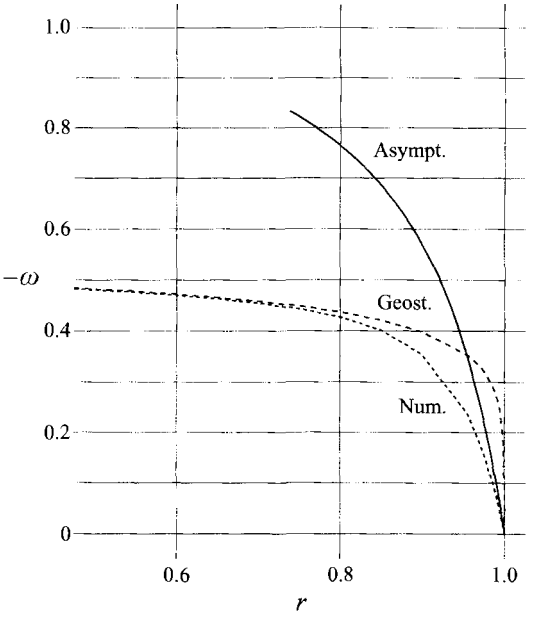

FIGURE 5. ω *vs.* r, $\varepsilon = 0.05$, $H = 5$, rigid sphere: geostrophic result (23), $E^{2/7}$ layer asymptotic approximation (41)–(42) for $s \leqslant 5$, and numerical solution of (16)–(18).

Indeed, from the analytical viewpoint, it turns out that the accuracy of the $E^{2/7}$ layer correction to the geostrophic flow on a sphere is restricted to considerably smaller values of ε than that of the $E^{1/4}$ layer on the disk. This must be emphasized, because it is counterintuitive. One is inclined to argue that the thickness of the boundary layer sets the restriction on the accuracy of the approximation. Therefore, since the $E^{2/7}$ layer is asymptotically thinner than the $E^{1/4}$ layer, the domain of validity of the $E^{2/7}$ layer approximation is expected to be larger than the domain of validity of the $E^{1/4}$ layer. This argument fails here due to a mathematical difficulty: while the $E^{1/4}$ layer for the disk is matched to the correct constant outer value ω_0, the $E^{2/7}$ layer for the sphere is matched (rather, patched) at $r = 1 - x_1$ to an approximation to the geostrophic flow which has an inherent relative error of about $(2x_1)^{1/4}$. Evidently, the outer solution of (39) is $-(2x)^{1/4}$, while the geostrophic flow (combine (23) with (37), or take the outer solution of (38)) is $\omega_0 = -(2x)^{1/4}[1 - (2x)^{1/4} + O(x^{1/2})]$. To get less than 10% discrepancy at the matching point we need $x_1 < 5 \times 10^{-5}$, i.e. $H^2E < 2.2 \times 10^{-18}$; for $H^2E > 3 \times 10^{-4}$ the approximation at x_1 deviates by more than 100%. Figure 5 illustrates the big overshoot of the approximation (39) for $\varepsilon = 5 \times 10^{-2}$ (i.e. $H^2E = 2.5 \times 10^{-5}$).

This difficulty can also be spotted at the stage of replacing (38) by (39), which requires the assumption that $(2x)^{-1/4} \geqslant (2x_1)^{-1/4} \gg 1$. Physically, this means that the inclination of the Ekman layer on the sphere is assumed so large that the Ekman layer on the non-inclined container wall, represented by the last term in the left-hand side of (38), can be neglected.

The $E^{2/7}$ layer accuracy requirement, say $H^2E < 10^{-18}$, is also consistent with the condition $(HE)^{1/3} \ll H^{4/7}E^{2/7}$, i.e. the $E^{1/3}$ shear layer is considerably thinner than the quasi-geostrophic layer.

However, in practical and experimental devices the typical values of H^2E are above 10^{-4}, hence the results for the $E^{2/7}$ layer theory are only of academic interest.

In other words, although the strength of the Ekman layer on the sphere is indeed increased due to the local inclination, this enhancement is really important only for $x = 1 - r \lesssim 10^{-4}$. For larger values of x the difference between the sphere and the disk geometry, from the point of view of the Ekman layer, is not significant and the flow field will probably tend to the $E^{1/4}$ shear layer arrangement if the $E^{2/7}$ layer is not sufficiently thin to be encompassed by the former region.

Reconsidering (38)–(41) we find that the approximation (39) is much improved if we add (rather, keep) the term $-\omega$ in the left-hand side of (39). The outer solution of the thus modified (39) is $-[1 + (2x)^{-1/4}]^{-1}$ which recovers the geostrophic flow within less than 10% for any $0 < x \leqslant 1$ (the original (39) requires $x < 5 \times 10^{-5}$ for such accuracy). However, we could not find a simple asymptotic solution of this improved equation, and when a numerical approach is considered the original (16) can be solved with the same effort.

3.3. *Numerical solutions*

The finite differences solution of the quasi-geostrophic equation (16) subject to the boundary conditions (17)–(18) was performed on a uniform mesh, see Appendix C. The reported results, with $\varepsilon \geqslant 0.05$, were calculated with mesh interval $\delta r = 1/400$, so that at least 20 mesh points were available in the sidelayer. The integration of (20) for obtaining D was performed by the rectangle rule. The accuracy was ascertained by the disk configuration, $f(r) \equiv 0$: the exact results (26) and (27) were recovered with four correct significant digits.

Figure 6 displays the profiles of ω *vs.* r on a rigid sphere. The influence of ε is very significant: the relative discrepancy with the geostrophic profile, $1 - \omega/\omega_0$, is, roughly, 1 at $r \approx 1$ and ε at $r \approx 1 - \varepsilon$. For $\varepsilon \geqslant 0.2$ the 'sidelayer' spreads into the entire core and ω on the axis is reduced; the profiles bear strong resemblance to the disk counterpart, see figure 3(*a*). Similar calculations (not shown) indicate that the above-mentioned features are only slightly modified when H increases from 5 to larger values: for $\varepsilon \leqslant 0.1$ the profiles are practically unchanged, and for $\varepsilon \geqslant 0.2$ the value of $|\omega(r)|$ is slightly reduced and the resemblance with the disk is enhanced. This influence of H can be readily inferred from (16).

The radial velocity in the core is $O(1)$ in the region where ω differs significantly from the geostrophic result, cf. (25).

The above-mentioned behaviour of ω is, as expected, reflected in the features of the drag force, D, as seen in figures 7 and 8. Figure 7 shows the influence of ε on the quasi-geostrophic drag on a rigid sphere: starting with the geostrophic value D_0 at $\varepsilon = 0$, an almost linear decrease to $0.5D_0$ as $\varepsilon = 0.2$ occurs; then, at slower rates of decrease, $0.2D_0$ and $0.1D_0$ are obtained for $\varepsilon \approx 0.5$ and 0.7, respectively.

Figure 8 displays the ratio D of a sphere to D_d (of a disk) *vs.* $\varepsilon[2/(1 + \kappa]^{1/2}$, for different no-slip parameters κ and particle to wall distance H. (The combination $\varepsilon[2/(1+\kappa]^{1/2}$ is used because this is the e-fold thickness of the 1/4 layer for a non-rigid particle, as indicated in §3.1. Recall that for rigid particles $\kappa = 1$.) This figure is connected with (27) (or figure 3(*b*)) which provides D_d for any $\varepsilon[2/(1 + \kappa]^{1/2}$. The presented results cover a wide range of configurations and can be used for comparison with experiments.

The conclusion is that, for a given κ, the ratio D/D_d is quite close to 1 for $\varepsilon[2/(1 + \kappa]^{1/2} > 0.1$ provided that $H \geqslant 10$. It should be emphasized that, in the range $0.1 \leqslant \varepsilon[2/(1 + \kappa]^{1/2} \leqslant 1$, D_d decreases by a factor of about 15. This confirms the strong analogy between the quasi-geostrophic flows on a disk and on a sphere when $\varepsilon[2/(1 + \kappa]^{1/2} > 0.1$, which was indicated by figures 6 and 3(*a*).

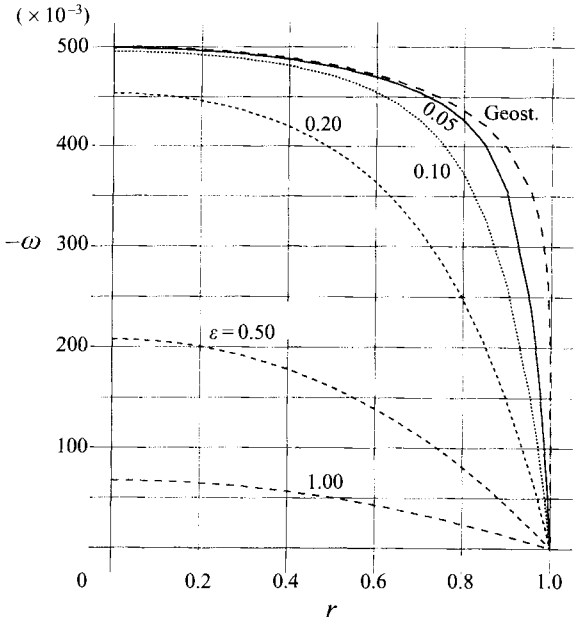

FIGURE 6. ω *vs.* r, for various ε, $H = 5$, rigid sphere.

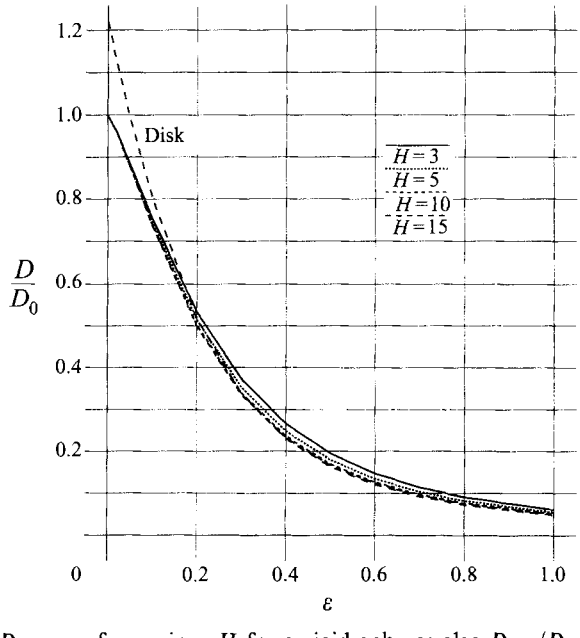

FIGURE 7. D/D_0 *vs.* ε, for various H for a rigid sphere; also $D_{disk}/D_{0\,sphere}$, labelled 'disk'.

4. Some inertial modifications

The setting $Ro = 0$, which was used in the foregoing sections, yields serious uncertainties about the validity of the results for small but non-zero values of Ro. Suppose we expand the flow-field variables in powers of Ro. The leading terms are given by the foregoing linear theory results. A subsequent order of magnitude

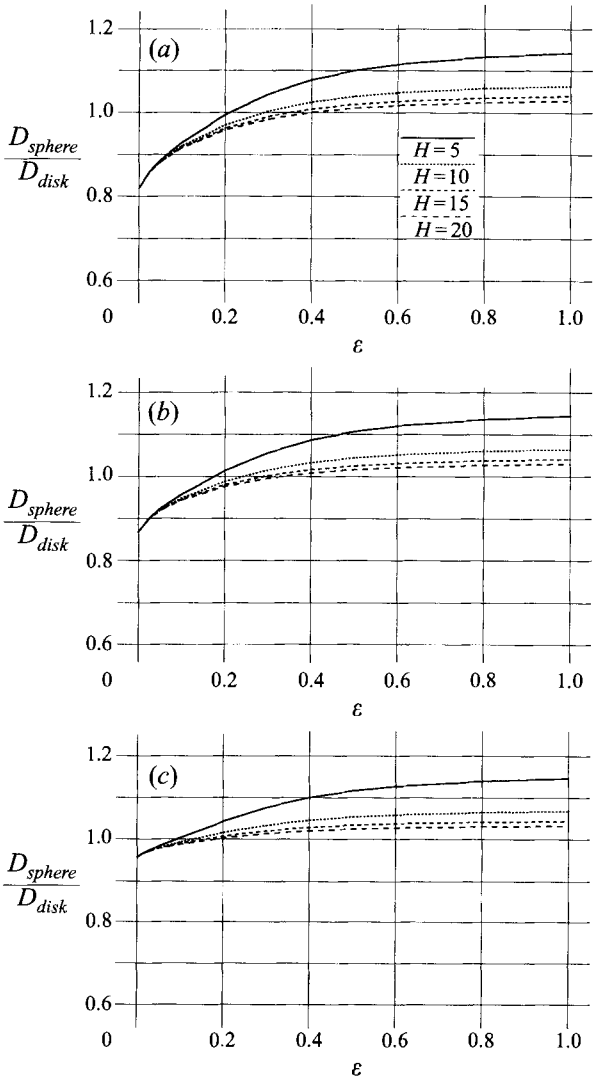

FIGURE 8. $D_{disk}/D_{0\,sphere}$ *vs.* $\varepsilon[2/(1+\kappa)]^{1/2}$, for various H and (*a*) $\kappa = 1$, (*b*) $\kappa = 0.5$, (*c*) $\kappa = 0.1$.

consideration of the terms of (5)–(7) indicates that, for small ε at least, the largest inertial terms appear in the shear regions associated with the shear term of (16).

This realization has been used in previous studies for estimating the 'effective' Rossby number as $RoE^{-a}H^{-b}$ and thus obtaining restrictions of the form $Ro \ll E^a H^b$ for the formal accuracy of the leading term (linear theory) results. In particular, in the azimuthal momentum balance (6), the term $Rou(\partial v/\partial r)$ is, formally, as important as the linear Coriolis term $2u$ when $Rov/\delta \sim RoE^{-1/2}\omega/\delta$ is of order unity, where the values of ω and of δ (the thickness of the shear layer) are provided by (16).

Moore & Saffman (1968), using for a sphere the estimates $\delta \sim \varepsilon^{8/7}$, $\omega \sim \varepsilon^{2/7}$, see (40)–(39), derived the restriction $Ro \ll E^{1/2}\varepsilon^{6/7} \approx E^{5/7}H^{3/7}$. Similarly, for a disk $\delta \sim \varepsilon$, $\omega \sim 1$ giving the even more restrictive $Ro \ll E^{1/2}\varepsilon \approx E^{3/4}H^{1/2}$.

The important question is: what are the leading inertial modifications, i.e. what happens to the flow field when Ro, although sufficiently small for keeping the linear

theory balances dominant, is nevertheless big enough for making some inertial terms quantitatively comparable with the Coriolis ones. This question has been considered for several rotating-fluid problems, e.g. Wedemeyer (1964), Hide (1968), Barcilon (1970), Bennets & Hocking (1973), Bennets & Jackson (1974), but, to the best of our knowledge, not for the present rising-particle configuration. The source–sink problems discussed in some of these papers have common points with the present flow, especially for a disk: the upper shear layer drains fluid from the Ekman layer into the $E^{1/3}$ sidelayer, like in a sink flow, and the opposite pattern occurs on the lower side of the particle, resembling a source flow (in view of the different scalings, the present Ro corresponds to $RoE^{-1/2}$ in the above papers). However, the existing results cannot be carried over to our problem because of the different geometry and the fact that we are interested in the influence of Ro on the drag force.

We proceed as follows. We assume that the Ekman layer transport (or 'suction') correlation is not affected by Ro in the range of investigation, and that the orders of magnitude of the flow-field variables with respect to E and H are like in the linear case. Therefore, keeping the largest terms in (5)–(6) yields for the quasi-geostrophic core the radial and the azimuthal momentum equations (recall, $v = \omega r E^{-1/2}$)

$$-2\omega r E^{-1/2}(1 + \tfrac{1}{2}RoE^{-1/2}\omega) = -E\frac{\mathrm{d}p}{\mathrm{d}r}; \tag{46}$$

$$2u\left[1 + \tfrac{1}{2}RoE^{-1/2}\left(r\frac{\partial\omega}{\partial r} + 2\omega\right)\right] = E^{1/2}\frac{\mathrm{d}}{\mathrm{d}r}\frac{1}{r}\frac{\mathrm{d}}{\mathrm{d}r}r^2\omega; \tag{47}$$

the axial momentum and continuity balances (13)–(14) are unchanged. Comparing (47) to (12) we conclude that the modified form of (16) is

$$2\frac{\varepsilon^2}{F(r)}\left[1 - \frac{f(r)}{H}\right]\left(\frac{\mathrm{d}^2\omega}{\mathrm{d}r^2} + \frac{3}{r}\frac{\mathrm{d}\omega}{\mathrm{d}r}\right) - \left[1 + \kappa(1 + f'^2)^{1/4}\right]\omega = \pm 1, \tag{48}$$

where the $-$ in the right-hand side is for the lower side of the particle,

$$F(r) = 1 + \tfrac{1}{2}RoE^{-1/2}\left(r\frac{\partial\omega}{\partial r} + 2\omega\right); \tag{49}$$

the boundary conditions are (17)–(18). Comparing (46) to (11) we find that the drag is given now by

$$D = 2\pi E^{-3/2}\int_0^1 \left|\omega_u(1 + \tfrac{1}{2}RoE^{-1/2}\omega_u) - \omega_l(1 + \tfrac{1}{2}RoE^{-1/2}\omega_l)\right| r^3\mathrm{d}r, \tag{50}$$

where u and l denote the upper and the lower sides of the particle.

The restriction on Ro now — but not the only one as discussed below — is $\frac{1}{2}RoE^{-1/2} \ll 1$. Otherwise the time-dependent terms in the momentum equations are significant and the steady (actually, quasi-steady) state assumed here cannot be attained from simple initial conditions (Ungarish 1996). Evidently, when $\frac{1}{2}RoE^{-1/2}$ approaches 1 the absolute angular velocity, $\Omega^*(1 + RoE^{-1/2}\omega)$, apparently approaches zero in the upper core and $2\Omega^*$ in the lower core, and such big changes from a basic solid-body rotation must be accompanied by a large mass (angular momentum) transfer, i.e. an $O(H)$ displacement of the particle.

Equation (48) must be solved by iteration. Since in the linear case ω is negative on the upper side and positive on the lower side, the factor (49) is anticipated to cause different qualitative behaviours in these regions. For the shear layers where

$\partial\omega/\partial r$ is dominant, when Ro increases we expect a thickening in the lower region and a contraction in the upper region (essentially, like near a source and a sink, respectively). Therefore in the nonlinear case the antisymmetry of ω with respect to z is lost, and we must use (50) instead of (20). The loss of symmetry also causes a rotation of the torque-free body, but this can be discarded, as justified later.

Some indicative profiles of the angular velocity are displayed in figure 9. Compared to the linear case, we observe the following changes due to the inertial terms. In the upper part the shear layer is thinner and $|\omega|$ in the core is smaller. In the lower part the shear layer is thicker and ω in the core is a bit larger; moreover, here we also notice a peculiar change of the slope near $r = 1$, which actually reflects the appearance of an inertial sublayer for sufficiently large Ro.

In this inertial sublayer the azimuthal Coriolis component is counterbalanced by convection of angular momentum. Indeed, it is easily verified that

$$\omega = (RoE^{-1/2})^{-1}\left(\frac{1}{r^2} - 1\right) \tag{51}$$

renders both sides of (47) equal to zero and satisfies the boundary condition $\omega(r = 1) = 0$. The radial velocity in the sublayer can be calculated from the volume balance,

$$u = \{-1 + [1 + \kappa(1 + f'^2)^{1/4}]\omega\}r/2H[1 - f(r)/H]. \tag{52}$$

We note that the angular velocity distribution (51) is stable with respect to Rayleigh's criterion, see Greenspan (1968, §6.2), hence no evident instability can be attributed to the inertial effects.

We can argue the following. (*a*) This sublayer is necessary when, taking the linear solution for ω on the lower side and the actual Ro of interest, the function $F(r)$ attains negative values. Hence it occupies at least the region where the thus-calculated $F(r)$ is negative. For a disk geometry and small ε this consideration, in view of (30), yields the thickness $\sim -\gamma\varepsilon \ln[2(1 + \kappa)\gamma\varepsilon/RoE^{-1/2}]$ which is evidently meaningful only for $RoE^{-1/2} > 2(1 + \kappa)\gamma\varepsilon$, i.e. $RoE^{-3/4} > 2(1 + \kappa)^{1/2}H^{1/2}$. However, for the sphere and other similar geometries the numerically calculated linear ω should be used in this evaluation. This predicts the thicknesses 0.02 and 0.10 for the sublayer in the cases of figures 9(*b*) and 9(*c*) respectively, in fair agreement with the calculated profiles of ω_l. (*b*) The maximal extent of the inertial layer is estimated by the intersection between (51) and the geostrophic ω_0. This yields, approximately, $0.25RoE^{-1/2}$ for a solid disk and $0.5(RoE^{-1/2})^{4/3}(1 - (4/3)(RoE^{-1/2})^{1/3})$ for a solid sphere (for $RoE^{-1/2} \ll 1$).

Now we proceed to the drag calculations via (50). It turns out that the quite complex influence of the inertial terms on the profiles of ω_u and ω_l almost counterbalance in the integral (50), hence the drag force decreases monotonically and quite mildly when Ro increases from 0 to $\sim 10E^{3/4}$. For example, for $E = 4 \times 10^{-5}$, $H = 5$, the drag force is $0.875E^{-3/2}$ and $0.796E^{-3/2}$ for $Ro = 0$ and 0.01, respectively ($RoE^{-3/4} = 0$ and 19.9); on the other hand, the corresponding geostrophic drag is $1.29E^{-3/2}$. The conclusion is that in the range of interest (say, $\varepsilon \sim 0.1$ and $Ro \lesssim 0.01$) the shear modifications of the geostrophic drag are more important than the inertial corrections.

Similar results were obtained for other values of E and Ro and are summarized in figure 10 as $D/(\pi E^{-3/2}/2)$ *vs.* $RoE^{-3/2}$, following the suggestion of Maxworthy (1968) (in particular, figure 3 there; the difference in values between the effective Rossby numbers $RoE^{-3/4}H^{-1/2}$ indicated by the disk, and $RoE^{-3/2}$ used for historical reasons, is not significant in the range of parameters under discussion). Typically, the results are about 30% below the geostrophic value at $Ro = 0$ and decrease further by

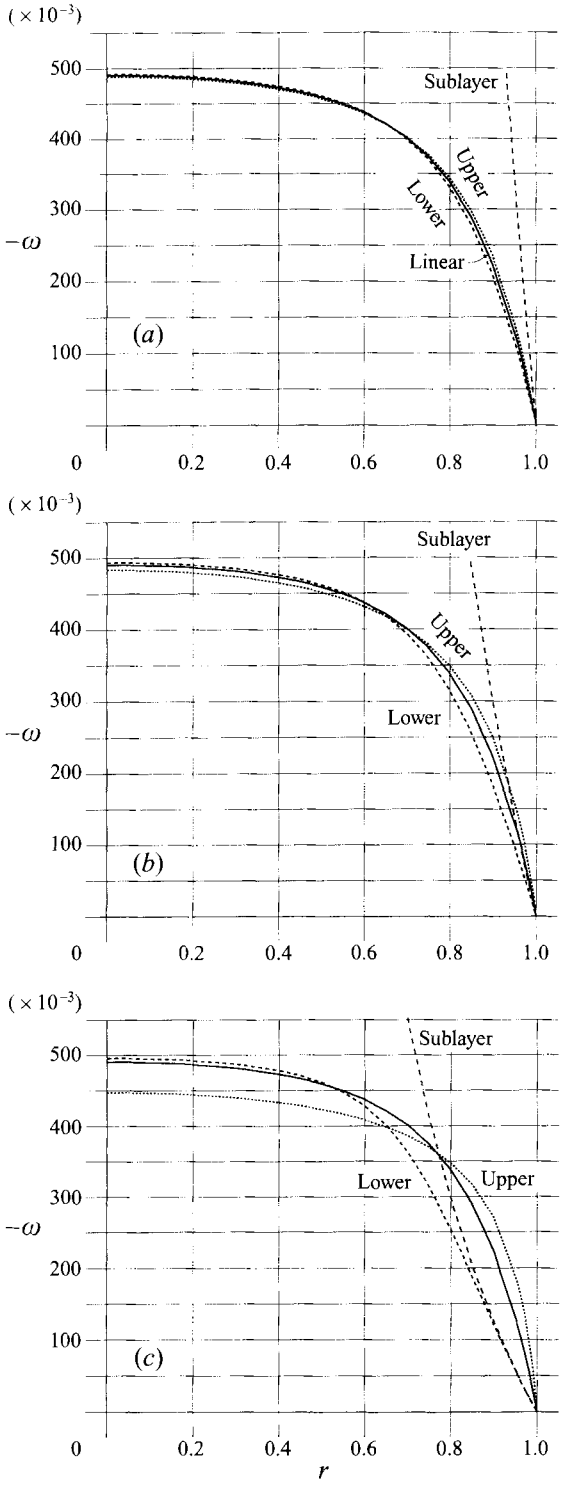

FIGURE 9. ω *vs.* r, the influence of Ro, rigid sphere. The upper, lower (with changed sign) and linear profiles are shown, together with the inertial sublayer approximation (51). $E = 0.4 \times 10^{-4}$, $H = 5$, and (*a*) $Ro = 0.002$, (*b*) $Ro = 0.005$, (*c*) $Ro = 0.012$.

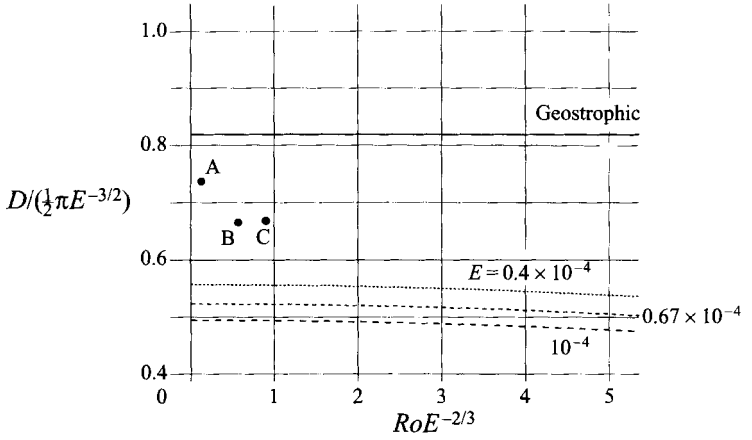

FIGURE 10. Drag *vs.* $Ro\,E^{-2/3}$, solid sphere, $H = 5$. The points are from Maxworthy (1968), see table 1 (points E,D,F are attributed to $H = 10.5$ and therefore not shown).

about 2% as the effective Rossby number $RoE^{-3/2}$ goes to 5 ($RoE^{-3/4} \sim 10$). Some experimental points are also shown in figure 10, to be discussed later.

The present inertial modifications of the linear theory are expected to be indicative when $\frac{1}{2}RoE^{-1/2} \ll 1$, but their accuracy is probably limited by two major factors.

First, the linear Ekman layer transport (or suction) correlation used in (48) requires quantitative corrections for larger Ro. Actually, when in the shear layer the inertial terms become as big as the Coriolis terms, the same is expected to happen in the Ekman regions, where the inertial modifications are complicated. Thus we estimate that the effective Rossby number is $\sim RoE^{-3/4}$ also in the Ekman layer. There are good indications that even when the effective Rossby number in the Ekman region is of order unity the linear correlation approximates well the integral transport feature (e.g. in the von Kármán and Bödewadt problems), but this still leaves the limitation $RoE^{-3/4} \lesssim 1$.

Second, the incorporation of the inertial terms breaks the flow-field symmetries with respect to $z = 0$, and begins to affect the validity of the boundary condition $\omega(r = 1) = 0$. The appearance of the inertial layer on the lower side is probably the limit of validity of that symmetric condition, which was derived from shear balance considerations.

Moreover, when the symmetry is violated a torque-free ($M = 0$) body will rotate, in contrast with the foregoing assumption. This rotation is, however, quite small when ε and Ro are of the orders of magnitude considered here. For a solid particle the angular velocity ω_p can be calculated from the dominant Ekman-layer friction torque formula,

$$M = 2\pi E^{-1} \int_0^1 [(\omega_u + \omega_l) - 2\omega_p] \frac{r^3}{(1+f'^2)^{1/4}} \mathrm{d}r = 0. \tag{53}$$

Since the difference between $-\omega_u$ and ω_l is pronounced in the shear layer of thickness $\delta \leqslant \varepsilon$ we expect from (53) $\omega_p = O[\delta \max(|\omega_u + \omega_l|)]$. The $\max(|\omega_u + \omega_l|)$ is proportional to Ro. It can therefore be estimated, using in (53) the values of ω_u and ω_l obtained without particle rotation, that when ε and $RoE^{-1/2}$ are small then ω_p is negative and considerably smaller than ω in the cores.

We speculate that this non-zero ω_p will have a secondary influence on the drag for the following reasons. Consider a symmetric geometrical configuration. The rotation

(without translation) of the particle does not create drag. For a rising non-rotating particle *in the linear case* the drag will not be affected if we add rotation (the additional angular velocities in the upper and lower cores are equal). Thus, the influence of ω_p on the drag of a rising particle is expected to enter only via the nonlinear influence of the additional rotation on the main flow field produced by the axial motion. To be more specific, the additional ω_p may further affect the factors $F(r)$ given by (49) in the upper and lower regions, thus enhancing the contraction and thickening of the corresponding Stewartson layers. Since this asymmetry of the Stewartson layers contributed up to about 2% to the drag in the previous calculations, it is expected that variations in this asymmetry, even if $O(1)$, will not contribute to the drag more than a few percent. (The leading term in (49), $\partial\omega/\partial r$, is large in the asymptotic sense for small ε, but in the practical cases, when $\varepsilon \sim 0.1$, the numerical absolute value of this term is smaller than 5.) We could not find a clear-cut argument for predicting the direction of this additional drag modification.

To substantiate these estimates we performed several more rigorous calculations not subjected to the symmetry assumptions. Some details and typical results are presented in Appendix D. It turns out that the rotation of the particle causes additional slight decrease of the drag, i.e. the discrepancy with the experiment increases.

5. Comparisons and discussion

Some useful conclusions of the foregoing analysis can be summarized. Taking $\varepsilon \sim 0.1$ and $H \gtrsim 5$ as typical, we find the following.

(i) The ratio of the quasi-geostrophic linear drag, D, to the geostrophic D_0 is lower than 1 by about 25% , and decreases with ε (i.e. E and/or H increase).

(ii) The ratios D/D_0 for a sphere and for a disk are close; this compatibility increases with ε and H.

(iii) The core flow in a quite wide region $0.7 < r < 1$ is affected by viscous effects and different from the geostrophic predictions. In particular, $|\omega/\omega_0| < 1$ and the radial motion has $u = O(1)$.

(iv) The inertial effects break the symmetry: the shear layer shrinks in the upper region ('forward wake') and thickens on the lower side ('rear wake') where also an inertial sublayer appears for $Ro \gtrsim E^{3/4}H^{1/2}$. However, the net drag force decreases by only about 1% when Ro changes from 0 to $\sim E^{3/4}$.

A clear-cut comprehensive verification of the present theory is not yet feasible. The available theoretical and experimental data are incomplete and/or deviate from the present set of assumptions in some respects, as follows.

The relevant theoretical 'exact' results given by Ungarish & Vedensky (1995) cover only the rigid disk geometry for $Ro = 0$ and $E \gtrsim 10^{-4}$ and do not always satisfy the assumption $(HE)^{1/3} \ll 1$. The comparison shows that the quasi-geostrophic model captures well the flow-field features outside the $E^{1/3}$ layer. However, in the verified range of $\varepsilon \sim 0.05$–0.7 the quasi-geostrophic drag, although giving the correct dependency on ε, was systematically below the exact value, see table 1 of Ungarish & Vedensky (1995) . This is attributed to the influence of the $E^{1/3}$ layers; indeed the discrepancy increases from 15% to 30% to 60% when $(HE)^{1/3}$ varies from 0.04 to 0.1 to 0.2, approximately. It is reasonable to infer a very similar behaviour for a spherical particle.

The relevant experiments are these performed by Maxworthy (1968) with solid spheres and Bush *et al.* (1995) with drops of various viscosities; the indicative values of the parameters are $E \sim 10^{-4}, Ro \sim 10^{-2}, H \sim 5$–$10$. These reports are extremely

$E \times 10^4$	$RoE^{-2/3}$	H	ε	$\frac{D}{D_0}$, test $\pm 2.5\%$	$\frac{D}{D_0}$, here	$\frac{D_{\text{here}}}{D_{\text{test}}} - 1$	$(HE)^{1/3}$	Label
0.40	0.1	5.15	0.128	0.90	0.68	−0.24	0.06	A
0.40	1.6	10.50	0.182	0.76	0.54	−0.29	0.07	
0.53	0.6	5.15	0.137	0.82	0.65	−0.21	0.06	B
0.53	1.3	10.50	0.196	0.77	0.51	−0.34	0.08	
0.67	0.9	5.15	0.145	0.82	0.63	−0.23	0.07	C
0.67	2.3	10.50	0.207	0.65	0.49	−0.25	0.09	

TABLE 1. Comparisons with experiments of Maxworthy (1968) (test). (Note: for these cases $E^{-3/4}/E^{-2/3} \approx 2.3$. The labels are used in figure 10)

useful for qualitative comparison, but on the quantitative side we encounter the following difficulties:

(*a*) Maxworthy (1968) did not label the measurement points with the value of H. According to the general description of the apparatus, H was 5.15 in some cases and 10.5 in others, but for comparison we need to know the value at the point under consideration.† Moreover, even for the smallest E and H in the covered range, $(EH)^{1/3} > 0.05$.

(*b*) The experiments of Bush *et al.* (1995) were performed at typical $E = 4 \times 10^{-4}$, therefore $(HE)^{1/3} > 0.13$ for $H \sim 5$–10. Owing to the drop release device the lower boundary of the container deviates from the assumption of a flat solid wall and is rather closer to a fluid–fluid interface (Bush (1993, p. 84)); it can be argued that this weakens the Ekman layer there and increases the drag. Furthermore, in the test the Bond number Σ was small, indicating spherical drops, but $g^*/\Omega^{*2}a^* \sim 25$. We assumed that this parameter is very small, otherwise the shape of the drop is not symmetric with respect to $z = 0$, see figure 15(*b*) of Bush *et al.* (1995). The resulting shape indicates an increase of drag, but we have no quantitative estimate for this effect.

In both experimental investigations the flow-field patterns were scrutinized, and the time of motion of a buoyant particle along a known interval was actually measured; the corresponding velocity, W^*, is proportional to $1/D$ (recall the scaling (4)). Maxworthy (1968) gives values of D (in various scaled forms), Bush *et al.* (1995) report values of W^* (scaled with the geostrophic rising velocity of a bubble). Both sources performed comparisons with the geostrophic model and concluded that, even for the smallest attained Ro, the drag is lower (the rising velocity is higher) than the predictions, and the flow field in the core displays some features (in particular, $O(1)$ radial velocity) that violate the expected pattern. These discrepancies with the geostrophic model were attributed to the neglected inertial terms, i.e. to the not sufficiently small Ro.

The present theoretical investigation indicates that the above-mentioned trends observed by Maxworthy (1968) and Bush *et al.* (1995) can – or rather should – be first attributed to the shear in the lateral Stewartson layers. In the experiments the value of ε was, typically, $0.1 - 0.2$. Figures 6 and 7 show that for such values of ε: (*a*) the linear quasi-geostrophic drag is about 30% lower than the geostrophic one; (*b*) the lateral shear layers are quite thick, therefore observable 'cores' of $O(1)$ radial

† Professor Maxworthy kindly searched his files for this information following the author's request, but could not retrieve it.

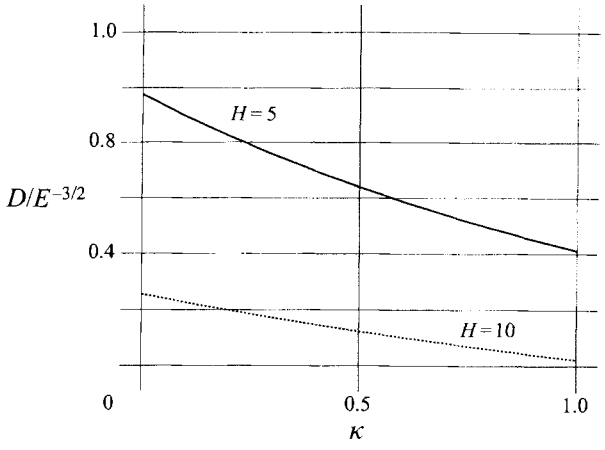

FIGURE 11. Drag *vs.* κ at $E = 0.4 \times 10^{-3}$, for the sphere and two values of H.

velocity are present, and ω differs from the geostrophic prediction even near the axis. Moreover, figure 10 suggests that, for constant H, the quasi-geostrophic $D/E^{-3/2}$ decreases when Ro and E increase. The same trends can be inferred from figure 3 of Maxworthy (1968) and figure 12 of Bush *et al.* (1995). Figure 7 here shows that D decreases when ε, i.e. $H^{1/2}$, increases if other parameters are unchanged. A similar behaviour is inferred from figure 11 of Bush *et al.* (1995), who also noticed that the rise speed (i.e. drag) is relatively insensitive to changes of β (i.e. κ). Again, good qualitative agreement exists: figure 11 here shows that the quasi-geostrophic drag in conditions relevant to the experiments decreases only by about 25% when κ varies from 0 to 1 (the geostrophic drag varies by about 60%, see figure 2).

Some quantitative comparisons with points extracted from figure 3 of Maxworthy (1968) are given in table 1 (for two values of H) and in figure 10 (for one value of H). It is emphasized that we have inferred the values of H of the points under the assumption that for the same E the larger value of H corresponds to the smaller D, but we have no independent confirmation for this choice. The geostrophic drag, D_0, overestimates the measured drag by about 25%. On the other hand, the present calculations underestimate the measured drag by about 25%, so that, in the strict sense, their accuracy is not superior. However, they predict the correct trend with respect to changes of the parameters in the experiment, while the geostrophic drag changes only with E. According to the present estimates, see figure 10, in the range of $RoE^{-2/3}$ of table 1 the contribution of the inertial terms to D is less than 1%. We therefore claim that the quantitative difference seen in table 1 and figure 10 between the experiments and the quasi-geostrophic calculations is not caused essentially by the neglect of the inertial terms. We attribute this discrepancy to the following factors. (*a*) The $E^{1/3}$ shear layers are not really thin. The contribution of these layers, as inferred from the disk geometry, is expected to increase the drag above the quasi-geostrophic value. We are presently unable to calculate this contribution for a sphere. (*b*) The measured D reflects an average over different positions of the particle, where the quasi-geostrophic drag force is expected to be, in general, larger than at the midway between the plates location assumed in the present theory. However, as indicated by calculations, see Appendix D, and by observations (T. Maxworthy 1995, personal communication), this is a small effect, perhaps within the range of the measurement error.

From figure 11 of Bush *et al.* (1995) the quantitative behaviour of D *vs.* ε can be extracted as follows: in our context, the vertical axis corresponds to $\pi E^{-3/2}/D$ (the numerator is the geostrophic drag on a bubble, see (22)), and the horizontal axis corresponds to $1/(2H)$. With the given $a^* = 2$ cm, and the general data of the experiment, we estimated $E \approx 4 \times 10^{-4}$. Also given, $\beta = 10$, i.e. $\kappa = 10/11$. Thus, figure 11 of Bush *et al.* (1995) shows that for $\varepsilon \approx 0.35$ (the smallest value of $1/(2H)$) $\pi E^{-2/3}/D \approx 4.1$, and for $\varepsilon \approx 0.2$ the result is $\pi E^{-2/3}/D \approx 3.0$. Our calculations, on the other hand, give $\pi E^{-3/2}/D = 8.5$ and 4.5 for these values of ε (note that $\pi E^{-3/2}/D_0 = 2.3$). The agreement in the trend of influence of ε is, again, correct – but the discrepancy in drag is big. However, for these parameters the $E^{1/3}$ layers are really thick, $(HE)^{1/3} \approx 0.12$ and 0.17, a fact that can explain a discrepancy of about 40%–60% in the observed direction. For the radial motion our calculations show that the variable $u(2H/r) = 1 - \omega/\omega_0$ increases from 0.5 to 1 when r increases from r_1 to 1, where $r_1 = 0.85$ for $\varepsilon = 0.2$ and $r_1 = 0.24$ for $\varepsilon = 0.35$.

Figure 10 of Maxworthy (1968) gives some measurements of ω_l and $|\omega_u|$ at $r \approx 0$ *vs.* RoE^{-1} for $0.63 \times 10^{-4} < E < 2.5 \times 10^{-4}$ (i.e. $0.14 < \varepsilon < 0.2$ and $0.2 < \varepsilon < 0.29$ for $H = 5.15$ and 10.5, respectively). The scatter is big, but ω_l is always above $|\omega_u|$ by several percent, and $0.5(\omega_l + |\omega_u|)$ varies from 0.45 to 0.3, approximately. This is in good agreement with the present theory, which predicts that, for that range of ε, $\omega(r \approx 0, Ro = 0)$ varies from 0.49 to 0.36, and that ω_l is above $|\omega_u|$ when $Ro > 0$, but $0.5(\omega_l + |\omega_u|)$ is just a bit below the linear results, see figures 6 and 9.

In spite of the low predictive accuracy for the drag force in the tested practical situations, the quasi-geostrophic drag model results are valuable because: (*a*) They describe correctly the variation of the drag with the parameter ε and apparently provide the lower limit of the linear drag, while D_0 gives the upper limit. (*b*) They rehabilitate the reliability of the linear theory, by indicating that the discrepancies reported by Maxworthy (1968) and Bush *et al.* (1995) are not a failure of the linear approach for $Ro \sim 10^{-3} - \sim 10^{-2}$, rather a result of the oversimplified treatment of the Stewartson layers in the derivation of D_0. Moreover, they indicate the modifications associated with the non-zero Rossby number. (*c*) They describe, at least qualitatively, the important transition region from the 'short'-container geostrophic case, $\varepsilon \to 0$, where D_0 applies, to the 'long'-container case, $\varepsilon > 1$, where $D \approx (\pi/24)E^{-2}/H$, see Hocking *et al.* (1979), Ungarish & Vedensky (1995).

However, both Maxworthy (1968) and Bush *et al.* (1995) reported some wavy streak-line patterns that apparently cannot be explained by the present slightly nonlinear steady-state model. Maxworthy (1968;1995, personal communication) suggests that these oscillations are manifestations of 'undular inertial waves', accompanied by an acceleration and a decrease of pressure of the flow after it has passed the equator into the lower region. Such a behaviour is likely to contribute a positive drag correction to the present results, but a quantitative estimate is not available. Oscillations may also indicate instability, so that the stability problem of these flows remains an important open question. The present results may serve as starting 'unperturbed' flow fields for stability analysis.

Extensions of the present model to additional configurations non-symmetric with respect to z, e.g. an upper free surface or drops not in the middle position, are possible but awkward, because the angular velocity of the torque-free particle (which is not a constant for drops) and the boundary condition $\omega(r = 1)$ are not known *a priori*. However, this is an interesting topic for further investigation, especially in the context of asymmetric drops, and the calculations presented in Appendix D are a first step in this direction.

It appears now that the main reason for the discrepancy between the available drag prediction model and the experiments (assuming the flow is stable) is the fact that $(EH)^{1/3}$ is not sufficiently small in the practical devices. New experiments, or numerical solutions of the full Navier–Stokes equations, in which this parameter is small, are necessary for verifications.

It is now more evident that for practical values of E and H the available asymptotic analysis of the linear problem (i.e. the classic combination of cores, Ekman boundary layers and Stewartson free shear layers) is not sufficiently accurate for drag predictions. Formally, this could be anticipated: in addition to the requirement that $(EH)^{1/3}$ is fairly small, the representative thickness ratio of the $E^{1/3}$ to the $E^{1/4}$ layers which is $(E/H^2)^{1/12}$ should also be small, but this is not satisfied in practical configurations ($(E/H^2)^{1/12} > 0.29$ in Maxworthy 1968); actually, a systematic expansion for a sphere would also require that $E^{1/21}$, and perhaps E at even smaller powers is very small, see Greenspan (1968, end of §2.18†). Nevertheless, one could hope that the actual contribution of the higher-order terms, beyond these included in (16), is small, especially for a spherical particle where the geostrophic angular velocity already satisfies the boundary conditions. The present study seems to exclude this possibility. This provides further motivation for attempting the solution of the complete linear problem for a sphere, either by analytical means (like Ungarish & Vedensky 1995 did for a disk, and the method used by Tanzosh & Stone 1994 for a sphere in the unbounded domain seems a good candidate) or by numerical means. The resulting drag force will most likely be in fair agreement with the available experiments at small Ro.

The author had illuminating discussions with Professors H. P. Greenspan, D. W. Moore, H. A. Stone and J. W. M. Bush. The research was partially supported by the Fund for the Promotion of Research at the Technion.

Appendix A. Brief derivation of (16)

Consider the configuration of figure 12 for $E \ll 1$ so that the Ekman layers are very thin.

The interface $\Sigma : z - f(r) = 0$ divides the embedding fluid (I) and the embedded particle (drop, bubble) (II). To return to the notation of the paper, the index (I) should be deleted and the index (II) replaced by $DROP$. In the cores the azimuthal velocities v_i ($i = I$ or II) are z-independent, and the azimuthal momentum equation gives

$$2u_i = E\frac{\mathrm{d}}{\mathrm{d}r}\frac{1}{r}\frac{\mathrm{d}}{\mathrm{d}r}rv_i, \tag{A 1}$$

hence $u_i = o(v_i)$ with respect to the small E, because the radial length scale is much larger than $E^{1/2}$.

The Ekman layers, assumed thin, on the top wall and on the interface match these cores to the boundary conditions: no-slip on solid wall, velocity and stress continuity on the interface. The layers above and below Σ have different thicknesses, $\sim (\nu_i^*/\Omega^*)^{1/2}$, therefore the ratio ν_I^*/ν_{II}^* plays a role in the analysis; since the stress involves $\mu_i^* = \nu_i^*\rho_i^*$, the ratio ρ_I^*/ρ_{II}^* also enters the results.

Let ζ be the local coordinate normal to the boundary, γ be the angle between $\hat{\zeta}$ and $\hat{z}$, and $\tilde{U}$ and $\tilde{v}$ denote the Ekman layer velocity *corrections* in the longitudinal

† There is a small misprint in the book: $E^{1/7}$ should be $E^{2/7}$.

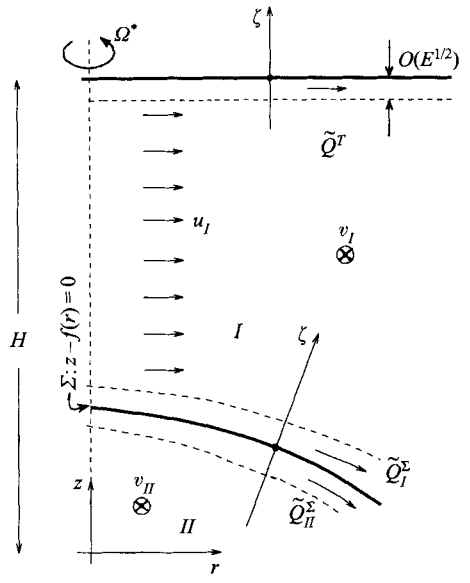

FIGURE 12. Sketch of the Ekman layers and cores (I outside the particle, II inside the drop).

and azimuthal directions, respectively. The Ekman-type balance between Coriolis and viscous terms in region $i = I, II$ can be expressed as

$$\frac{v_i^*}{\Omega^* a^{*2}} \frac{\partial^2}{\partial \zeta^2}(\tilde{U} + \mathrm{i}\tilde{v}) - 2\mathrm{i}\cos\gamma(\tilde{U} + \mathrm{i}\tilde{v}) = 0, \tag{A 2}$$

where $\mathrm{i} = \sqrt{-1}$ and, again, the asterisk denotes dimensional variables.

It is convenient to introduce the stretched coordinate:

$$\tilde{\zeta} = \frac{\zeta^*}{(v_I^*/\Omega^*)^{1/2}} = \frac{\zeta}{E^{1/2}},$$

and notice that (A 2) has solutions of the form $C \exp\left[\pm(1+\mathrm{i})(\cos\gamma)^{1/2}(\frac{v_I^*}{v_i^*})^{1/2}\tilde{\zeta}\right]$.

The particular solutions $\tilde{U} + \mathrm{i}\tilde{v}$ corresponding to the configuration of figure 12 are

$$-\mathrm{i}v_I \exp\left[(1+\mathrm{i})\tilde{\zeta}\right] \quad \text{on the top wall;} \tag{A 3}$$

$$\mathrm{i}(v_{II} - v_I)\kappa \exp\left[-(1+\mathrm{i})(1+f'^2)^{-1/4}\tilde{\zeta}\right] \quad \text{above the interface;} \tag{A 4}$$

$$-\mathrm{i}(v_{II} - v_I)\frac{\kappa}{\beta} \exp\left[(1+\mathrm{i})(1+f'^2)^{-1/4}\left(\frac{v_I^*}{v_{II}^*}\right)^{1/2}\tilde{\zeta}\right] \quad \text{below the interface;}$$

where

$$\beta = (\rho_{II}^*/\rho_I^*)(v_{II}^*/v_I^*)^{1/2}, \quad \kappa = \beta/(1+\beta).$$

The volume transport in these layers, in the longitudinal direction, is given by $\tilde{Q} = \mathrm{Re}\{E^{1/2}\int_{\tilde{\zeta}_{min}}^{\tilde{\zeta}_{max}}(\tilde{U} + \mathrm{i}\tilde{v})\mathrm{d}\tilde{\zeta}\}$, therefore

$$\tilde{Q}_I^T = -\tfrac{1}{2}E^{1/2}v_I, \quad \tilde{Q}_I^\Sigma = -\tfrac{1}{2}E^{1/2}(v_I - v_{II})(1+f'^2)^{1/4}\kappa \tag{A 5}$$

($\tilde{\zeta}_{min}$ is $-\infty$ or 0, and $\tilde{\zeta}_{max}$ is 0 or ∞, according to the location of the layer with respect to $\zeta = 0$). Consider now the volume balance in the cylinder of radius r closed by the

upper wall and by the interface. The wall moves towards the interface with velocity 1, thus pushing fluid radially outwards via the Ekman layers and the core,

$$\pi r^2 \times 1 = 2\pi r \left[\tilde{Q}_I^T + \tilde{Q}_I^\Sigma + u_I[H - f(r)]\right]. \tag{A 6}$$

We substitute (A 5) and (A 1). If the configuration is symmetric with respect to z, then $v_{II} = 0$ is necessary for counterbalancing the $\tilde{Q}_{II}^\Sigma$ flux on the mirror image of Σ. In this case, letting $v_I = E^{-1/2}\omega r$, we obtain, after some arrangement, (16).

For a solid particle the continuity conditions on Σ are replaced by the usual no-slip conditions. This leaves (A 3) unchanged, but in (A 4) κ should be replaced by 1.† On the other hand, for an inviscid particle (bubble) no Ekman layer appears on Σ. This leaves, again, (A 3) unchanged, but in (A 4) κ should be replaced by 0. This indicates that, for the flow outside the particle, the results (A 5) are reliable for $0 \leqslant \kappa \leqslant 1$. However, if the flow inside the drop is of interest, the validity of the core–Ekman layer decomposition there becomes invalid if $(v_{II}^*/\Omega^*)^{1/2}/a^* > 0.1$, say. The viscous limit of the internal flow is discussed by Bush *et al.* (1995)

If v_I and v_{II} are known (A 6) provides the radial velocity in the core, u_I. In particular, for $v_{II} = 0$ and $v_I = E^{-1/2}\omega r$ we get in core I

$$u = \{1 + [1 + \kappa(1 + f'^2)^{1/4}]\omega\} r/2H[1 - f(r)/H]. \tag{A 7}$$

We introduce the stream function ψ defined by $ru = \partial\psi/\partial z$ with value 0 on the particle. On account of (A 5) and (A 7) this can be expressed as

$$\psi = \frac{r^2}{2}\left(\{1 + [1 + \kappa(1 + f'^2)^{1/4}]\omega\}\frac{z - f(r)}{H - f(r)} - \kappa(1 + f'^2)^{1/4}\omega\right), \tag{A 8}$$

for $f^+(r) < z < H^-$, $0 < r < 1$. The last term is the contribution of the Ekman layer on the particle. We note in passing that $\psi = -\frac{1}{2}r^2$ on the upper wall whose axial velocity is -1, while (A 8) gives for $z = H^-$ a different value due to the Ekman layer on that wall. The axial velocity outside the Ekman layers is given by

$$w = -\frac{1}{r}\frac{\partial\psi}{\partial r}. \tag{A 9}$$

Appendix B. The solution of (41)–(42)

The numerical solution of

$$G''(s) - G(s)/s^{1/4} = -1, \quad s \geqslant 0,$$

with $G(0) = 0, G(s)/s^{1/4} = 1$ for $s \to \infty$, encounters obvious difficulties for $s \to 0$. Therefore, we use standard numerical initial-value problem solvers for $s \geqslant 0.01$, and for smaller s we introduce the expansion

$$G(s) = G'(0)\left[s + a_1 s^{11/4} + a_2 s^{9/2} + \cdots\right] - \left[\tfrac{1}{2}s^2 + b_1 s^{15/4} + b_2 s^{11/2} + \cdots\right]. \tag{B 1}$$

Substitution in the equation gives the coefficients $a_1 = 16/77, b_1 = 8/165, a_2 = 960/72765, b_2 = 224/114345$. The value $G'(0) = 1.013292$ is found by shooting from $s = 0.01$ to match the boundary conditions for large s. We note that (B 1) gives $G(0.5)$ with four correct digits and $G(1)$ with three correct digits.

† For a solid particle v_{II}/r must be a constant. This is consistent with $v_{II} = 0$ here.

Appendix C. Finite-difference formulation of (16)

We introduce the grid with interval $\delta r = 1/N$, the staggered grid,

$$r_i = \delta r(i - \tfrac{1}{2}),\ i = 0, 1, ..., N + 1, \tag{C 1}$$

and use central differences approximations to replace (16) by

$$q_i \left[\frac{1}{\delta r^2}(\omega_{i+1} - 2\omega_i + \omega_{i-1}) + \frac{3}{2r_i\delta r}(\omega_{i+1} - \omega_{i-1})\right] - S_i\omega_i = 1,\ i = 1, 2, ...N; \tag{C 2}$$

with

$$\omega_0 = \omega_1;\ \omega_{N+1} = -\omega_N; \tag{C 3}$$

(here the index 0 does not mean the geostrophic approximation), where

$$q_i = 2\varepsilon^2[1 - f(r_i)/H]; \tag{C 4}$$

$$S_i = 1 + \kappa(1 + f'^2(r_i))^{1/4}. \tag{C 5}$$

This yields a standard three-diagonal system for the unknowns $\omega_1, \omega_2 \cdots \omega_N$ which we solve by direct elimination.

For the nonlinear modification (48)–(49) we define q_i as the right-hand side of (C 4) divided by $F(r_i)$, and solve this nonlinear version of (C 2) by iterations, starting with $\omega_i^{(0)}$, until convergence of $\omega_i^{(k)}/\omega_i^{(k-1)}$ for all i is achieved. The linear ω_i turns out to be a good choice for $\omega_i^{(0)}$. However, the iterations for the lower side begin to diverge for some larger values of Ro; continuation from one converged case to one with larger Ro improved the range of convergence.

Appendix D. Some results with asymmetric conditions.

The symmetry simplifications of the model may be violated by the geometry of the configuration and by the inertial terms that affect differently the upper and lower regions. Here we attempt to incorporate the asymmetric effects of off-middle particle position and of the inertial modifications in the shear layers. The evident results in the flow field are that the particle acquires an angular velocity and the outer region $r > 1$ is also set in motion.

Consider a symmetric *solid* particle whose equatorial plane is at distance H_u from top the plate and H_l from the bottom plate, such that

$$H_u + H_l = 2H = H_O.$$

We distinguish between the upper (top), lower (bottom) and outer cores, denoted by u, l and O, respectively. The torque-free particle rotates with ω_p. The equations of motion, cf. (48)–(49), are now

$$2\frac{\varepsilon_s^2}{F_s(r)}\left[1 - \frac{f(r)}{H_s}\right]\left(\frac{\mathrm{d}^2\omega_s}{\mathrm{d}r^2} + \frac{3}{r}\frac{\mathrm{d}\omega_s}{\mathrm{d}r}\right) - [1 + (1 + f'^2)^{1/4}]\omega_s = R_s,\ 0 \leqslant r \leqslant 1,\ s = u, l; \tag{D 1}$$

$$2\frac{\varepsilon_O^2}{F_O(r)}\left(\frac{\mathrm{d}^2\omega_O}{\mathrm{d}r^2} + \frac{3}{r}\frac{\mathrm{d}\omega_O}{\mathrm{d}r}\right) - 2\omega_O = 0,\ r \geqslant 1; \tag{D 2}$$

where

$$\varepsilon_s = \left(\frac{1}{2}H_s\right)^{1/2} E^{1/4} = \left(\frac{H_s}{H}\right)^{1/2} \varepsilon, \quad s = u, l, O; \tag{D 3}$$

$$R_u = -1 + (1 + f'^2)^{1/4}\omega_p, \quad R_l = 1 + (1 + f'^2)^{1/4}\omega_p. \tag{D 4}$$

The boundary conditions, following Moore & Saffman (1969) , are

$$\frac{\mathrm{d}\omega}{\mathrm{d}r} = 0 \text{ at } r = 0, \ \omega_u = \omega_l = \omega_O \text{ at } r = 1, \tag{D 5}$$

$$\omega_O = 0 \text{ at } r \to \infty, \tag{D 6}$$

$$H_u \frac{\mathrm{d}\omega_u}{\mathrm{d}r} + H_l \frac{\mathrm{d}\omega_l}{\mathrm{d}r} = H_O \frac{\mathrm{d}\omega_O}{\mathrm{d}r} \text{ at r} = 1. \tag{D 7}$$

In addition, the torque on the particle, see (53), must vanish.

We solved the system by the finite-differences method outlined in Appendix C, imposing the $\omega_O = 0$ condition at $r = 2$. We note in passing that for the sphere configuration the last term on the left-hand side of (D1) behaves like $\omega[2(1-r)]^{-1/4}$ near $r = 1^-$ and now, in contrast with the symmetric case, $\omega(r = 1) \neq 0$. The use of the staggered grid (C1) takes proper account of this difficulty without special adjustments. From the analytical point of view, see Appendix B, this is reproduced by the addition of terms $G(0)[1+(16/21)s^{7/4}+...]$ in the solution of the sidelayer (B1) when the boundary condition $G(0) \neq 0$ is imposed, where G is defined as $(-\omega+\omega_p)/B$, see (40).

Some results are presented below, table 2(*a–d*) for a disk and a sphere, at the middle and two off-middle positions, in the linear and slightly nonlinear ($Ro = 0.003$) cases. The other parameters are fixed as

$$E = 0.4 \times 10^{-4}, \quad H = 5 \text{ (i.e. } \varepsilon = 0.126).$$

These calculations support the conjecture that the middle-position symmetric conditions for the particle are relevant for the understanding of the drag force behaviour in practical circumstances. Indeed, when these simplifications are removed the variation of the drag is about 10 times smaller than the deviation from the geostrophic D_0 introduced by the incorporation of the shear layers.

This confirms the expected hierarchy of effects on the drag: the major contribution is from the geostrophic ω_0; the major correction to the geostrophic drag comes from the thick Stewartson shear layers in the region $1 - \varepsilon < r < 1$, as calculated in the symmetric ($H_u = H_l$) linear ($Ro = 0$) case; the correction to the thickness of these shear layers comes from the asymmetry ($H_u \neq H_l$ and/or $Ro > 0$). Thus, the asymmetry effects can be regarded as a correction to the correction to the geostrophic drag, and, in the range of parameters tested here, are rather small.

The range $H_u/H = 0.5$–1.5 covers most of the test section in Maxworthy's experiments: the central 25 cm of a container of 40 cm. The observed velocity – hence drag – was almost constant in this region (Maxworthy 1995, personal communicaiton; recall that the experimental accuracy was estimated as $\pm 2.5\%$). This can be considered as experimental support for the conjecture that the middle position drag has global relevance.

The value of $RoE^{-2/3}$ covers the experimental cases used for comparison, see table 1.

We note that the dependency of $(D/D_0 - 1)$ on H_u/H_l, for a disk at small ε and $Ro = 0$, was estimated by Ungarish & Vedensky (1995, Appendix B, and in particular

	(a)			(b)		
H_u/H	1.5	1	0.5	1.5	1	0.5
ω_p	0.038	0.000	−0.038	−0.036	−0.067	−0.11
$\omega(r=1)$	−0.041	0.000	0.041	−0.12	−0.080	−0.048
D	0.967	0.924	0.967	0.912	0.877	0.907
D/D_0-1	−0.38	−0.41	−0.38	−0.42	−0.44	−0.42
	(c)			(d)		
H_u/H	1.5	1	0.5	1.5	1	0.5
ω_p	0.034	0	−0.034	−0.019	−0.048	−0.081
$\omega(r=1)$	−0.036	0	0.036	−0.102	−0.065	−0.034
D	0.909	0.875	0.909	0.871	0.841	0.867
D/D_0-1	−0.29	−0.32	−0.29	−0.32	−0.35	−0.33

TABLE 2. Some results for disks and spheres at the middle and two off-middle positions: (*a*) disk, $Ro = 0$; (*b*) disk, $Ro = 0.003$ (i.e. $RoE^{-1/2} = 0.47$, $RoE^{-2/3} = 2.56$; (*c*) sphere, $Ro = 0$; (*d*) sphere, $Ro = 0.003$.

equation (B30)). Table 2(*a*) and other similar results not shown here are in good agreement with that estimate.

Remark: If we estimate the drag at the middle position with inertial correction while still assuming $\omega_p = 0$ and $\omega(r = 1) = 0$, we obtain $D/D_0 - 1 = -0.42$ for the disk and −0.33 for the sphere, quite close to the more accurate values given in tables 2(*b*) and 2(*d*).

REFERENCES

BARCILON, V. 1970 Some inertial modifications of the linear viscous theory of steady rotating fluid flows. *Phys. Fluids* **13**, 537–544.

BARNARD, B. J. S. & PRITCHARD, W. G. 1975 The motion generated by a body moving through a stratified fluid at large Richardson numbers. *J. Fluid Mech.* **71**, 43–64.

BENNETS, D. A. & HOCKING, L. M. 1973 On nonlinear Ekman and Stewartson layers in a rotating fluid. *Proc. R. Soc. Lond.* A **333**, 469–489.

BENNETS, D. A. & JACKSON, W. D. N. 1974 Source-sink flow in a rotating annulus: a combined laboratory and numerical study. *J. Fluid Mech.* **66**, 689–705.

BUSH, J. W. M. 1993 Drop motion in rotating fluids: a model of compositional convection in the earth's core. PhD thesis, Harvard University, Cambridge, MA, USA.

BUSH, J. W. M., STONE, H. A. & BLOXHAM, J. 1992 The motion of an inviscid drop in a bounded rotating fluid. *Phys. Fluids* A **4**, 1142–1147.

BUSH, J. W. M., STONE, H. A. & BLOXHAM, J. 1995 Axial drop motion in rotating fluids. *J. Fluid. Mech.* **282**, 247–278.

GREENSPAN, H. P. 1968 *The Theory of Rotating Fluids*. Cambridge Uniersity Press.

HIDE, R. 1968 On source-sink flows in a rotating fluid. *J. Fluid Mech.* **32**, 737–764.

HOCKING, L. M., MOORE, D. W. & WALTON, I. C. 1979 The drag on a sphere moving axially in a long rotating container. *J. Fluid Mech.* **90**, 781–793.

MAXWORTHY, T. 1968 The observed motion of a sphere through a short, rotating cylinder of fluid. *J. Fluid Mech.* **31**, 643–655.

MOORE, D. W. & SAFFMAN, P. G. 1968 The rise of a body through a rotating fluid in a container of finite length. *J. Fluid Mech.* **31**, 635–642.

MOORE, D. W. & SAFFMAN, P. G. 1969 The structure of free vertical shear layers in a rotating fluid and the motion produced by a slowly rising body. *Trans. R. Soc. Lond.* A **264**, 597–634.

STEWARTSON, K. 1966 On almost rigid rotations. *J. Fluid Mech.* **26**, 131–144.

TANZOSH & STONE 1994 Motion of a rigid particle in a rotating viscous flow: An integral equation approach. *J. Fluid. Mech.* **275**, 225–256.

UNGARISH, M. 1996 Some spin-up effects on the geostrophic and quasi-geostrophic drag on a slowly rising particle in a rotating fluid, submitted.

UNGARISH, M. & VEDENSKY, D. 1995 The motion of a rising disk in a rotating axially bounded fluid for large Taylor number. *J. Fluid Mech.* **291**, 1–32.

WEDEMEYER, E. H. 1964 The unsteady flow within a spinning cylinder. *J. Fluid Mech.* **20**, 383–399.